DOE/ET-53088-572 IFSR #572

Kinetic Toroidal Ion Temperature Gradient Instability in the Presence of Sheared Flows

J.Q. DONG[a] AND W. HORTON
Institute for Fusion Studies
The University of Texas at Austin
Austin, Texas 78712

September 1992

[a] *Southwestern Institute of Physics, Leshan, China*

Kinetic Toroidal Ion Temperature Gradient Instability in the Presence of Sheared Flows

J.Q. Dong[a] and W. Horton
Institute for Fusion Studies
The University of Texas at Austin
Austin, Texas 78712

Abstract

The gyrokinetic integral equations for the study of the ion temperature gradient driven mode (η_i-mode) in toroidal geometry, at low plasma pressure, are extended to include equilibrium ion parallel $v_{0\|}(r)$ and perpendicular $v_E(r)$ sheared flows, where r is the minor radius of the flux surface. Magnetic gradient and curvature drifts of the ions as well as finite ion Larmor radius effects are included. The parallel sheared flow is shown to be destabilizing. The perpendicular sheared flow is a stabilizing mechanism. Mixing length estimates show that the η_i-mode induced ion thermal transport increases with increasing parallel flow shear, and decreases with perpendicular flow shear. The decrease of the ion transport is due not only to the decrease of the mode growth rate but also to the shrinking of the mode width. Using the mixing length formulas for the thermal transport associated with the unstable modes we show that the results are consistent with the experimental observations concerning the improvement of confinement in H-mode discharges coincident with the increase of cross-field sheared flows.

[a]Permanent address: Southwestern Institute of Physics, Leshan, China

I. Introduction

Experimental observations[1–3] and theoretical studies[4–6] indicate that the ion temperature gradient (ITG) driven drift wave instability is the most plausible candidate responsible for the anomalous ion thermal transport in tokamak plasmas although there are still some issues that need to be cleared up to make a final conclusion. Recent experimental results show[7–11] that stabilization of edge turbulence by nonuniform radial electric field $E_r(r)$ with the related $\mathbf{E} \times \mathbf{B}$ sheared flows is a potential explanation for the confinement improvement seen at the L to H transition. Motivated by those new facts several authors have studied the correlation between η_i-mode (ITG mode) and perpendicular flow shear.[12–14] Hamaguchi and Horton[12] show from fluid theory in a sheared slab geometry that ITG driven turbulent thermal transport is significantly reduced in the presence of sufficiently strong sheared poloidal flows. With kinetic considerations stability studies[13–14] show that poloidal sheared flow has a significant stabilization effect on the linear η_i-mode in slab geometry under the approximation that the mode wavelength is much longer than the ion gyroradius so that the finite ion Larmor radius effects are weak. In addition, it is indicated[13] that the results obtained with kinetic theory are significantly different from those obtained with the fluid approach.

In the early 70s[15] stability analysis showed that radial shear of the parallel velocity can drive microinstabilities in an inhomogeneous plasma with a sheared magnetic field. Motivated by the observations that significant levels of radially sheared toroidal flows have been measured in neutral-beam-heated discharges the effects of such flows on the slab η_i-mode are studied and found to be destabilizing.[13] The toroidal flow is essentially a parallel ion mass flow $v_{0\|}(r)$ in tokamaks. At the same time, parallel sheared flow is studied in an attempt to explain the edge turbulence recently.[16]

It has long been known that the finite Larmor radius effect is important for drift-type microinstabilities such as η_i-mode in plasmas of interesting parameters. In addition it is realized recently[17] that ion curvature and magnetic gradient drifts, which are neglected in slab geometry studies, have substantial destabilization effects on ITG driven mode and that the theoretical results after taking into account such effects are closer to the experimental measurements than the slab results are.

The integral equations which take into account full ion dynamics such as finite Larmor radius effects, curvature and magnetic gradient drifts $\omega_D(v_{||}^2, v_\perp^2, \theta)$ as well as parallel transit $k_{||}v_{||}$ relevant to the η_i-mode in toroidal geometry[17] are extended to include equilibrium ion parallel $v_{0||}(x)$ and perpendicular $v_E(x)$ sheared flows in this work, where $x = r - r_0$ with r being the variable in the minor radius direction and r_0 the minor radius of the mode rational surface. So-called quasi-toroidal model[17] in which the ion curvature and magnetic gradient drifts are taken to be constant over a flux surface and equal to the maximum values at $\theta = 0$ (the outside of the torus), and the mode coupling introduced due to the toroidal feature of the equilibrium magnetic configuration is neglected for simplicity. This means that the driving force for the instability is overestimated for most parameter regimes except when the mode width $\Delta\theta \geq \pi/2$ and magnetic shear $\hat{s} = rdq/qdr \geq 1$.[17] In this parameter regime the mode coupling has strong destabilization effects so that the quasi-toroidal model underestimates the mode growth. Fortunately, the errors introduced by the quasi-toroidal model are negligible for most of the parameter regimes presented in this work. The ion bounce motion and trapped ion effects are neglected due to less relevant to η_i-mode and electrons are considered to be adiabatic for simplicity.

In the stability analysis we introduce the six dimensionless parameters $\hat{v}'_E = (L_n/v_{ti})dv_E/dx$, $\hat{v}'_{0||} = (L_n/v_{ti})dv_{0||}/dx$, $\hat{L} = L_n/L_s$, $\eta_i = L_n/L_{Ti}$, $\epsilon_n = L_n/R$, $\tau_e = T_e/T_i$ and show the parametric dependence of $\gamma L_n/v_{ti} = f(\hat{v}'_E, v'_{0||}, \eta_i, \hat{L}, \epsilon_n, \tau_e, k_\theta\rho_i)$ and other numerical results, where L_n and L_{Ti} are the density and ion temperature gradient scale length, respectively,

L_s is the magnetic shear scale length, $v_{ti} = (2T_i/m)^{1/2}$ the ion thermal velocity and R the major radius of the torus.

The remainder of this work is organized as follows. In Sec. II the equilibrium distribution function of the ions in the presence of sheared flows are obtained and some approximations made to simplify the problem are discussed. The integral equation in the presence of sheared flows is derived and discussed in Sec. III and the numerical results are presented in Sec. IV. Section V is devoted to the discussions and conclusions of this study including comparisons with the experimental data on sheared flow.

II. Equilibrium Distribution Function in the Presence of Sheared Flows

The local velocity distribution functions in the presence of parallel sheared flow are Maxwellian distributions with a shift in the velocity component $v_{||}$ in the magnetic field direction. Detailed derivation of the particle distribution function in the presence of perpendicular sheared flow can be found in literature.[18] Here, only the outlines are given for the convenience of discussion.

The equation of motion of a charged particle in an electric field $E(x)\hat{\mathbf{x}}$ and magnetic field $\mathbf{B}(x)$ is given by

$$\frac{d^2\mathbf{r}}{dt^2} = \frac{e}{m} E(x)\hat{\mathbf{x}} + \Omega \mathbf{v} \times \hat{\mathbf{b}} \tag{1}$$

where $\mathbf{v} = d\mathbf{r}/dt$, $\Omega = eB/mc$ is the particle gyrofrequency, and e, m and B are the charge, mass and the ambient magnetic field, respectively, c is the speed of light in vacuum; $\hat{\mathbf{x}}$ is the unit vector in the x direction and $\hat{\mathbf{b}}$ in the magnetic field direction. The constants of motion are (i) the total energy related to perpendicular particle motion, $\alpha = (v_x^2 + v_y^2)/2 + e\Phi_0(x)/m$ with $E(x) = -\partial\Phi_0(x)/\partial x$; (ii) the thermal energy due to parallel motion, $\beta = (v_{||} - v_{0||}(x))^2/2$; and (iii) the position of particle guiding center $X_g = x + [v_y - v_E(X_g)]/\Omega$,

where $v_E(X_g) = -cE(X_g)/B$.

The general form of the distribution function of the charged particles in the presence of the electric field $E(x)\mathbf{x}$, magnetic field $\mathbf{B}(x)$ and parallel flow shear $v_{0||}(x)$ can be written as[18]

$$f_0(\alpha, \beta, X_g) = \frac{n(X_g)}{\pi^{3/2}\, v_t^3}\, g(X_g) \exp\left[-\frac{(v_x^2 + v_y^2)}{v_t^2} - \frac{(v_{||} - v_{0||})^2}{v_t^2} - \frac{e\Phi_0(x)}{T(X_g)}\right] \tag{2}$$

where $v_t = (2T(X_g)/m)^{1/2}$ is the thermal velocity of the charged particles, and $g(X_g)$ is a function determined by the normalization condition $\int f_0\, d\mathbf{v} = n$.

By expanding

$$\Phi_0(x) = \Phi_0(X_g) + \frac{d\Phi_0}{dx}(x - X_g) = \Phi_0(X_g) + \frac{Bv_E^2}{c\Omega} - \frac{Bv_E\, v_y}{c\Omega}$$

and substituting it into Eq. (2), the equilibrium distribution function in the presence of sheared flows is obtained as follows:

$$f_0(\alpha, \beta, X_g) = \frac{n(X_g)}{\pi^{3/2}\, v_t^3} \exp\left[-\frac{v_x^2 + (v_y - v_E)^2)}{v_t^2} - \frac{(v_{||} - v_{0||})^2}{v_t^2}\right] \tag{3}$$

where $v_E = v_E(X_g)$, $v_{0||} = v_{0||}(X_g)$ and

$$g(X_g) = \frac{n(X_g)}{\pi^{3/2}\, v_t^3} \exp\left[e\Phi(X_g)/\frac{1}{2}mv_t^2 + \frac{v_E^2}{v_t^2}\right] \tag{4}$$

has been obtained from the normalization condition mentioned above. We note that all the terms of order $\epsilon = v_E'(X_g)/\Omega$ or higher are neglected, compared with unity, for simplicity. Physically, this means that only weak perpendicular flow shear is considered here. Those high order terms have to be kept if instabilities such as the Kelvin-Helmholtz (KH) instability driven by strong shear in the flow velocity are considered. For such cases the equilibrium distribution function is complicated. However, the procedures presented in this work are still valid but become more complicated.

III. Integral Equation in the Presence of Sheared Flows

We consider a slab magnetic configuration $\mathbf{B} = B_0\left(\hat{\mathbf{z}} + \frac{x}{L_s}\hat{\mathbf{y}}\right)$, where L_s is the scale length of magnetic shear. The ion drift motion due to magnetic curvature and grad-B is taken to be $v_D = (v_\perp^2/2 + v_\parallel^2)/\Omega R$ over a flux surface, the value at $\theta = 0$ point, where R is the major radius of the magnetic configuration and θ is the poloidal angle.

By linearizing the distribution function $f = f_0 + f_1$ and substituting it into Vlasov equation, the perturbation of the distribution function is obtained,

$$f_1(x,\mathbf{v}) = -\frac{e}{T}\left\{ f_0\tilde{\phi}(x) + \left[i(\omega - \mathbf{k}\cdot\mathbf{v}_d)f_0 - i\frac{k_\theta T}{m\Omega}\frac{\partial f_0}{\partial X_g}\right]\right.$$
$$\left. \times \int_{-\infty}^{t} \tilde{\phi}(x')\exp\left[-i\omega(t'-t) + ik_\theta(y'-y) + ik_z(z'-z))\right]dt'\right\} \qquad (5)$$

where $\mathbf{v}_d = \mathbf{v}_E + v_{0\parallel}\,\hat{\mathbf{b}}$.

From the particle motion equation given by Eq. (1) it is easy to see that $\dot{v}_x = \Omega(v_y - v_E)$, or $\dot{v}_x = \Omega u_y$, and $\dot{u}_y = -\Omega v_x$ with $u_y = v_y - v_E(X_g)$ where the dot is the derivative with respect to time. Introducing $w_\perp^2 = v_x^2 + u_y^2$, $\tau = t' - t$, and $\delta' = \delta + \Omega\tau$, the phase of the particle gyromotion at the time t', then Eq. (5) may be written for the ions as

$$f_1(x,\mathbf{v}) = -\frac{e}{T_i}\left\{ f_0\tilde{\phi}(x) + \left[i(\omega - \mathbf{k}\cdot\mathbf{v}_d)f_0 - i\frac{k_y T_i}{m\Omega}\frac{\partial f_0}{\partial X_g}\right]\right.$$
$$\times \int_{-\infty}^{0} d\tau\tilde{\phi}(x')\exp\left[-i(\omega - k_\theta v_E - k_\parallel v_{0\parallel})\tau - \frac{i\epsilon_n\omega_{*e}}{\tau_e}\left(\frac{w_\perp^2\tau}{v_{ti}^2} + \frac{v_E^2\tau}{v_{ti}^2}\right.\right.$$
$$\left.\left. + \frac{2w_\perp v_E}{v_{ti}^2\Omega}(\cos\delta' - \cos\delta) + 2\frac{v_\parallel^2\tau}{v_{ti}^2}\right) + i\frac{k_\theta w_\perp}{\Omega}(\sin\delta' - \sin\delta)\right]\left.\right\}, \qquad (6)$$

where

$$f_0(\alpha,\beta,X_g) = \frac{n(X_g)}{\pi^{3/2}\,v_{ti}^3(X_g)}\exp\left[-\frac{w_\perp^2}{v_{ti}^2(X_g)} - \frac{(v_\parallel - v_{0\parallel}(X_g))^2}{v_{ti}^2(X_g)}\right], \qquad (7)$$

$\epsilon_n = L_n/R$ with L_n being the density gradient scale length, $\omega_{e*} = (k_y cT_e)/(eB\,L_n)$ is the electron diamagnetic drift frequency, and v_{ti} is the ion thermal velocity. From Eq. (7) it is

straightforward to obtain,

$$\frac{\partial f_0}{\partial X_g} = \left\{ \frac{n'}{n} + \frac{T_i'}{T_i} \left(\frac{w_\perp^2}{v_{ti}^2} - \frac{3}{2} + \frac{(v_\parallel - v_{0\parallel})^2}{v_{ti}^2} \right) + v_{0\parallel}' \frac{m(v_\parallel - v_{0\parallel})}{T_i} + v_E' \frac{m u_y}{T_i} \right\} f_0 \qquad (8)$$

with the prime " ' " being the derivative with respect to X_g.

The Fourier component of the perturbation of ion density is

$$\widehat{n}_i(k) = \frac{1}{\sqrt{2\pi}} \int \tilde{n}_i(x) \exp[-ikx] dx = \frac{1}{\sqrt{2\pi}} \int \exp[-ikx] dx \int f_1 \, d\mathbf{v} \ , \qquad (9)$$

and electrons are adiabatic

$$\widehat{n}_e(k) = \frac{en}{T_e} \widehat{\phi}(k) \ , \qquad (10)$$

where $\widehat{\phi}(k)$ is the Fourier component of the perturbed electrostatic potential.

Substituting Eq. (6) into Eq. (9) gives

$$\widehat{n}_i(k) = -\frac{ne}{T_i} \widehat{\phi}(k) - \frac{ie}{T_i} \int \frac{dk'}{\sqrt{2\pi}} \widehat{\phi}(k') \int \frac{dx}{\sqrt{2\pi}} \exp\left[i(k'-k)x\right] \int_{-\infty}^{0}$$
$$\times \exp\left[-i\omega\tau + ik_y v_E \tau - i \frac{\epsilon_n v_E^2}{\tau_e v_{ti}^2} \omega_{*e} \tau \right] H(\tau, x) d\tau \ , \qquad (11)$$

where $\tau_e = T_e/T_i$ and

$$H(\tau, x) = \frac{n}{\pi^{3/2}} \int d\widehat{v}_\parallel \, d\widehat{w}_\perp^2 \, d\delta \, J_0 \left(\frac{w_\perp k_\perp}{\Omega} \right) J_0 \left(\frac{w_\perp k_\perp'}{\Omega} \right) F$$
$$\times \exp\left[-(\widehat{u}_\parallel^2 + \widehat{w}_\perp^2) + ik_\parallel v_\parallel \tau - i \frac{\epsilon_n}{\tau_e} \omega_{*e} \tau (\widehat{w}_\perp^2 + 2\widehat{v}_\parallel^2) \right] \ , \qquad (12)$$

with

$$F = \omega_{*e} \left[\widehat{\omega} - \frac{k_\parallel v_{0\parallel}}{\omega_{*e}} - \frac{k_y v_E}{\omega_{*e}} + \frac{1}{\tau_e} + \frac{\eta_i}{\tau_e} \left(\widehat{w}_\perp^2 - \frac{3}{2} + \widehat{u}_\parallel^2 \right) - 2\widehat{v}_{0\parallel}' \widehat{u}_\parallel - 2\widehat{u}_y \widehat{v}_E' \right] \ , \qquad (13)$$

where $\eta_i = L_n/L_{T_i}$ with L_{T_i} being the ion temperature gradient scale length, $\widehat{\omega}$ is normalized to ω_{*e}, $\widehat{w}_\perp$, $\widehat{u}_\parallel$, $\widehat{v}_{0\parallel}$, $\widehat{v}_\parallel$ are normalized to v_{ti}.

The integrations over velocity space in Eq. (12) can be carried out analytically and give

$$H(\tau,x)=\frac{2n\omega_{*e}}{\sqrt{a}(1+a)}\Gamma_0(k_\perp,k'_\perp)\exp\left[-c+\frac{b^2}{4a}\right]\left\{\widehat{\omega}-\frac{k_\parallel v_{0\parallel}(x)}{\omega_{*e}}-\frac{k_y v_E(x)}{\omega_{*e}}\right.$$

$$+\frac{1}{\tau_e}+\frac{\eta_i}{\tau_e}\left[\frac{2}{1+a}F_0-\frac{3}{2}+\frac{1}{2a}+\left(\left(\frac{1}{a}-1\right)\widehat{v}_{0\parallel}(x)+\frac{ik_\parallel v_{ti}}{2a}\tau\right)^2\right]$$

$$\left.-\frac{2\widehat{v}'_{0\parallel}}{\tau_e}\left[\left(\frac{1}{a}-1\right)\widehat{v}_{0\parallel}(x)+\frac{ik_\parallel v_{ti}}{2a}\tau\right]\right\} \tag{14}$$

where

$$c=\widehat{v}_{0\parallel}^2=\frac{v_{0\parallel}(x)^2}{v_{ti}^2}\ ,$$

$$b=-(2\widehat{v}_{0\parallel}+ik_\parallel v_{ti}\tau)\ ,$$

$$a=1+\frac{i2\epsilon_n}{\tau_e}\omega_{*e}\tau\ ,$$

$$F_0=1-\frac{k_\perp^2+k_\perp'^2}{2(1+a)}+\frac{k_\perp k'}{(1+a)}\frac{I_1}{I_0}\ .$$

Sheared flows $v_E(x)$ and $v_{0\parallel}(x)$ are expanded and the terms of higher derivatives are neglected,

$$v_E(x)=v_E(0)+v'_E x\ ,$$

$$v_{0\parallel}(x)=v_{0\parallel}(0)+v'_{0\parallel}x=v_0+v'_{0\parallel}x\ .$$

Substituting Eq. (14) into Eq. (11) and performing the Fourier integration analytically gives the ion density perturbation in Fourier space. Then the Fredholm homogeneous integral equation of second kind can be obtained from quasi-neutrality condition as the mode dispersion equation

$$(1+\tau_e)\widehat{\phi}(k)=\int_{-\infty}^{+\infty}\frac{dk'}{\sqrt{2\pi}}K(k,k')\widehat{\phi}(k') \tag{15}$$

where

$$K(k,k') = -i\int_{-\infty}^{0} \omega_{*e} d\tau \frac{\sqrt{2}\,\exp\left[-i\left(\widehat{\omega}_0 + \frac{\epsilon_n}{\tau_e}\frac{v_E^2(0)}{v_{ti}^2}\right)\tau\omega_{*e}\right]}{\sqrt{a}\,(1+a)\sqrt{\lambda}} \cdot \exp\left[-\Theta^2 - \left(1-\frac{1}{a}\right)\widehat{v}_0^2\right]\left\{\widehat{\omega}_0\,\tau_e - \right.$$

$$\frac{i2\sqrt{a}\,\tau_e}{\tau\omega_{*e}}\left(\widehat{v}_0 + \frac{\widehat{v}'_E\,L_n}{(L_n/L_s)}\right)\Theta + 1 - \frac{3}{2}\eta_i + \frac{2\eta_i}{(1+a)}\left[1 - \frac{k_\perp^2 + k'^2}{2(1+a)\tau_e} + \frac{k_\perp\,k'_\perp}{(1+a)\tau_e}\frac{I_1}{I_0}\right] +$$

$$+\ \eta_i\left[\left(\frac{1}{a}-1\right)\left(\left(\frac{1}{a}-1\right)\widehat{v}_0^2 - \frac{2\widehat{v}_0}{\sqrt{q}}\Theta + \frac{1}{a}\Theta^2\right)\right] - \widehat{v}'_{0\|}\,L_n\left[\left(\frac{1}{a}-1\right)\widehat{v}_0 - \frac{1}{\sqrt{a}}\Theta\right]\left.\right\}\Gamma_0(k_\perp, k'_\perp)\,, \tag{16}$$

with

$$\Theta = \frac{k-k'}{2\sqrt{\lambda}} + \frac{\widehat{v}_{0\|}}{\sqrt{a}} + \frac{v'_E\,L_n\sqrt{a}}{(L_n/L_s)}\,,$$

$$\lambda = \frac{\tau^2}{\tau_e a}\left(\frac{L_n}{L_s}\right)^2 \omega_{*e}^2\,,$$

$$\widehat{\omega}_0 = \frac{\omega - k_y\,v_E(0)}{\omega_{*e}}\,, \tag{17}$$

$$\Gamma_0 = I_0\left(\frac{k_\perp\,k'_\perp}{(1+a)}\right)\exp\left[-(k_\perp^2 + k_\perp'^2)/2(1+a)\right]\,,$$

$$k_\perp^2 = k_\theta^2 + k^2\,, \qquad k_\perp'^2 = k_\theta^2 + k'^2\,,$$

k, k' and k_θ are normalized to $\rho_i^{-1} = \Omega/v_{ti}$ and x and X_g to ρ_i, and $I_j (j = 0, 1)$ is the modified Bessel function of order j.

The flat density profiles ($L_n \to \infty$) are not considered in this work so that the mode frequency is normalized to the electron diamagnetic frequency ω_{*e} and the time integral variable τ is normalized to ω_{*e}^{-1} in the equations. No essential changes are needed in Eqs. (16) and (17) except for rearranging those normalizations if flat density profiles are considered. Usually L_{Ti} instead of L_n is used for normalization in flat density profile cases.

It is easy to note that all the terms having $\widehat{v}_0$ vanish in slab limit ($a = 1$) except for the terms in Θ. The vanishing terms come from the ion curvature drift while the nonvanishing

terms come from magnetic shear $\left(v_{0\|}\, k_\| = v_0 \frac{k_\theta x}{L_s}\right)$ because parallel sheared flow instead of toroidal flow is considered here. Hereafter the flow velocities $v_0 = v_E(0) = 0$ are used since the emphasis is put on the effects of the flow shears. In this case the effects of a parallel sheared flow and a toroidal sheared flow should be the same.

Equation (16) is an extension of the formalism of Eq. (18) in Ref. 17 to include parallel and perpendicular sheared flows. By putting $\widehat{v}'_{0\|} = \widehat{v}_0 = \widehat{v}'_E = \widehat{v}_E(0) = 0$ we find that Eq. (16) reduces exactly to Eq. (18) in Ref. 17.

Another interesting case for Eq. (16) is the slab limit. If we put $a = 1$, which means that $L_n/R = 0$, in Eq. (14) and substitute the results into Eq. (11) then we have

$$\widehat{n}_i(k) = -\frac{e}{T_i}\left[n\widehat{\phi}(k) + \int \frac{dk'}{\sqrt{2\pi}}\,\widehat{\phi}(k') \int \frac{dx}{\sqrt{2\pi}}\,\exp\left[i(k'-k)x\right] S(x,k,k')\right] \tag{18}$$

where

$$S = i\int_{-\infty}^{0} d\tau \exp\left[-i\omega\tau + ik_y\, v_E\tau\right]\cdot n\omega_{*e}\,\Gamma_0 \exp\left[-\widehat{v}_{0\|}^2 + \frac{1}{4}\left(2\widehat{v}_{0\|} + ik_\|\, v_{ti}\tau\right)^2\right]\left\{\widehat{\omega} - \frac{k_\|\, v_{0\|}(x)}{\omega_{*e}}\right.$$

$$\left. -\frac{k_y\, v_E(x)}{\omega_{*e}} + \frac{1}{\tau_e} + \frac{\eta_i}{\tau_e}\left[F_0 - \frac{3}{2} + \frac{1}{2} - \left(\frac{k_\|\, v_{ti}}{2}\tau\right)^2\right] - \frac{2\widehat{v}'_{0\|}\, L_n}{\tau_e}\left(\frac{ik_\|\, v_{ti}}{2}\tau\right)\right\}$$

$$= n\Gamma_0\,\omega_{*e}\left\{\left[\frac{\omega_0}{\omega_{*e}} + \frac{1}{\tau_e} + \frac{\eta_i}{\tau_e}(F_0 - 1)\right]\frac{1}{k_\|\, v_{ti}}\, Z(\zeta_i) + \frac{\eta_i}{\tau_e}\frac{1}{k_\|\, v_{ti}}\left[\zeta_i - \frac{1}{2}Z(\zeta_i)\right.\right.$$

$$\left.\left. + \zeta_i^2 Z(\zeta_i)\right] - \frac{2\widehat{v}'_{0\|}L_n}{\tau_e}\,\frac{1}{k_\|\, v_{ti}}[1 + \zeta_i Z(\zeta_i)]\right\},$$

with

$$\zeta_i = \frac{\omega - k_\|\, v_{0\|} - k_y v_E}{k_\|\, v_{ti}},$$

and $Z(\zeta_i)$ is the plasma dispersion function. Finally, considering electrons as adiabatic we have the dispersion equation in slab case,

$$(1+\tau_e)\widehat{\phi}(k) = \int \frac{dk'}{\sqrt{2\pi}}\,\widehat{\phi}(k')K(k,k')\,, \tag{19}$$

where

$$K(k,k') = -\int_{-\infty}^{+\infty} \frac{dx}{\sqrt{2\pi}} \exp\left[i(k'-k)x\right] \left\{ \zeta_i Z(\zeta_i)\tau_e + \frac{\omega_{*e}}{k_{||} v_{ti}} \left[Z(\zeta_i) + \eta_i \left(\left(-b_1 + bI_1/I_0 - \frac{1}{2} \right) Z(\zeta_i) \right.\right.\right.$$

$$\left.\left.\left. + \zeta_i (1 + \zeta_i Z(\zeta_i)) \right) - 2\widehat{v}'_{0||} L_n (1 + \zeta_i Z(\zeta_i)) \right] \right\} \Gamma_0(k_\perp, k'_\perp) \tag{20}$$

$$b = \frac{k_\perp k'_\perp}{2} , \qquad b_1 = \frac{k_\perp^2 + k_\perp'^2}{4} . \tag{21}$$

In the shearless case $k_{||}, v_{0||}$, and v_E are all constant then Eq. (19) can be further simplified to the local dispersion equation,

$$1 + \tau_e \left[1 + \Gamma_0(k_\perp)\zeta_i Z(\zeta_i) \right] + \frac{\omega_{*e}}{k_{||} v_{ti}} \left\{ Z(\zeta_i)\Gamma_0 + \eta_i \left[\zeta_i + \left(\zeta_i^2 - \frac{1}{2} \right) Z(\zeta_i) \right] \Gamma_0 \right.$$

$$\left. - \frac{\eta_i}{2\tau_e} k_\perp^2 Z(\zeta_i) \left[\Gamma_0(k_\perp) - \Gamma_1(k_\perp) \right] \right\} + \frac{2\omega_{*e}}{k_{||} v_{ti}} \widehat{v}'_{0||} \left(1 + \zeta_i Z(\zeta_i)\right) = 0 , \tag{22}$$

which is equivalent to Eq. (35) in Ref. 13.

It is easy to realize from Eq. (22) that v_E does not change the stability of the mode but causes a Doppler shift of the mode real frequency relative to the laboratory frame in the local approximation since v_E enters the equation only through ζ_i. Such frequency shift is a function of x and will certainly change the particle-wave resonance and then the stability of the mode in the nonlocal case. This mechanism is analogous to the magnetic shear stabilization. The difference is that the wave-particle resonance parameter ζ_i changes through $k_{||}(x)v_{ti}$ in the magnetic shear stabilization while it does through $k_y v_E(x)$ in the poloidal flow shear stabilization.

Besides introducing a Doppler shift in the mode real frequency relative to the laboratory frame as v_E does, $v_{0||}$ has an extra effect on the mode, which is presented by the last term in Eq. (22). It is this term which makes the effects of the parallel flow shear on the η_i-mode completely different from that of the perpendicular flow shear. Here an attempt is made

to show the effect of this term. In the long wavelength regime, $k_\perp \rho_i < 1$, Eq. (22) can be written as a second order differential equation which is discussed in detail and numerically solved for a variety of parameter regimes in Ref. 13. In the fluid limit, $\zeta_i \gg 1$, and $v_E = 0$ case this second order differential equation reduces to

$$\frac{d^2\phi}{dx^2} - b_s\phi + \frac{1-\widehat{\omega}}{\widehat{\omega}+(1+\eta_i)/\tau_e}\,\phi + \left[\frac{(L_n/L_s)^2x^2}{\widehat{\omega}^2} + \frac{v'_{0\|}L_n(L_n/L_s)x}{c_s(\widehat{\omega}+(\eta_i+1)/\tau_e)\widehat{\omega}}\right]\phi = 0 \qquad (23)$$

where $b_s = k_\theta^2\rho_s^2$, $\widehat{\omega} = \omega/\omega_{*e}$, and x is normalized to $\rho_s = c_s/\Omega = \sqrt{T_e}/\sqrt{m_i}\Omega$. The dispersion relation obtained from Eq. (23) is

$$(k_\theta^2\rho_s^2+1)\widehat{\omega}^2 + \left[-1 + k_\theta^2\rho_s^2(1+\eta_i)/\tau_e + i\left(\frac{L_n}{L_s}\right)(2n+1) + \frac{v'^2_{0\|}\,L_n^2/4c_s^2}{\widehat{\omega}+(\eta_i+1)/\tau_e}\right]\widehat{\omega}$$

$$+ i\left(\frac{L_n}{L_s}\right)(2n+1)(1+\eta_i)/\tau_e = 0\ . \qquad (24)$$

It is easy to notice that the parallel flow shear effect on the instability is independent of the sign of the derivative of the flow $v'_{0\|}$. One approximate solution is that for $k_\theta^2\rho_s^2\,\frac{(1+\eta_i)}{\tau_e} \ll 1$ and $v'^2_{0\|}L_n^2/c_s^2 \lesssim 4(1+\eta_i)$

$$\widehat{\omega} \simeq \frac{i\,L_n\tau_e/L_s(2n+1)(1+\eta_i)}{1-\frac{v'^2_{0\|}\,L_n^2}{4c_s^2(1+\eta_i)}}\ . \qquad (25)$$

The condition $|v'_{0\|}|L_n/c_s(1+\eta_i)^{\frac{1}{2}} \lesssim 1$ is satisfied except in regions of strong $v'_{0\|}$ and flat density profile. From Eq. (25) we see that the last term of Eq. (22) has a destabilizing effect on η_i-mode. The numerical solutions of Eq. (24) given in Fig. 2 show the destabilization mechanism for a general parameter regime. Such a destabilization mechanism is due to the coupling between ion parallel transit motion and the radial shear of the parallel flow $v'_{0\|}$. The mechanism is very similar to the η_i destabilization mechanism but with ion temperature gradient replaced by the radial shear of the parallel flow. Because of this it is not surprising to find out numerically that instability is still possible for $\eta_i \simeq 0$ if $|v'_{0\|}| \gtrsim (1-2)v_{ti}/L_n$ (see Sec. IV) which can be satisfied for flat density profiles or strong flow shear.

IV. Numerical Results

A computer code is written to solve the integral eigenvalue equation Eq. (15) with the kernel given by Eq. (16). The main difference from the case without sheared flows[17] is that the symmetry properties such as $K(k,k') = K(k',k)$ and $\widehat{\phi}(k) = \widehat{\phi}(-k)$ which exist and significantly reduce the number of kernel evaluations in the case without flows are broken by the presence of equilibrium flows $v_{0\|}(x)$ and $v_E(x)$. This symmetry breaking increases the required computer time by about 4 times for getting an eigenvalue and an eigenfunction. Nonuniform grids are used to reduce the computer time needed without an appreciable decrease of accuracy.

A. Parallel Sheared Flow Effects

We first study the parallel sheared flow effects on the η_i-mode by putting $v_E(x) = 0$ in Eq. (15). The normalized mode growth rate $\gamma k_\theta \rho_i/\omega_{*e} = (\gamma L_n/c_s)\sqrt{2/\tau_e}$ versus poloidal wavenumber of the mode $k_\theta \rho_i$ is given in Fig. 1 for $\widehat{v}'_{0\|} = \frac{L_n}{v_{ti}} \frac{dv_{0\|}}{dx} = 0.0, 0.2$ and 0.5. It is seen that for the parameters studied here the parallel flow shear is always destabilizing over all unstable $k_\theta \rho_i$ region. At the same time the maximum growth rate remains at $k_\theta \rho_i \sim 0.7$ regime regardless of the parallel sheared flow. The mode real frequency is essentially not changed by such small parallel sheared flow.

The growth rate of the mode is given as a function of parallel flow shear in Fig. 2 for $\epsilon_n = 0.0$, 0.1 and 0.25. Destabilization effects induced by the ion curvature and magnetic gradient drifts are clearly shown and such destabilizing mechanism does not change in the presence of parallel sheared flow. However, the differences between the three growth rates seem to decrease with increasing of $\widehat{v}'_{0\|}$ which means that the parallel sheared flow destabilization effect slightly decreases with ϵ_n, the toroidicity parameter in the quasi-toroidal model approximation. Also shown in Fig. 2 are the solutions of Eq. (24), the dispersion equation

for the fluid approximation in sheared slab. The mode growth rate obtained from the fluid approximation is about five times higher than the kinetic result. The destabilization effect of the parallel sheared flow is independent of the sign of $\widehat{v}'_{0||}$ so that the curves are symmetric with respect to the vertical axis and only the results for $\widehat{v}'_{0||} \geq 0$ are presented.

The mode growth rate and real frequency versus η_i are presented in Fig. 3 for $\widehat{v}'_{0||} = 0,\ 0.5,$ 1.0, and 2.0. It is easy to notice in Fig. 3(a) that the parallel flow shear not only increases the η_i-mode growth rate but also decreases the threshold value of η_i. Even for $\eta_i = 0$ the instability is still possible if $v'_{0||}$ is large enough ($v'_{0||} \gtrsim 1.5 v_{ti}/L_n$). The mode growth rate for $\eta_i = 0$, $\widehat{v}'_{0||} = 2$ is the same as that for $\eta_i = 2.2$, $\widehat{v}'_{0||} = 0$ for the parameters used here. This may provide comparison between the free energy sources related to the temperature gradient and the parallel sheared flow. These results are different from the results obtained for the long wavelength mode in the slab,[13] which show that parallel sheared flow does not change the threshold value of η_i although it increases the mode growth rate when the mode is away from the marginal stability. The corresponding real frequency of mode is given in Fig. 3(b) which shows that the frequency increases with parallel sheared flow.

B. Perpendicular Sheared Flow Effects

The perpendicular flow shear v'_E effect on η_i-mode is shown in Fig. 4. It is seen that perpendicular sheared flow has stabilization effect on η_i-mode over all wavenumbers in the unstable spectrum except for the short wavelength region $k_\theta \rho_i \geq 1.2$. The dimensionless perpendicular flow shear $\widehat{v}'_E$ needed to have a notable stabilizing effects on the mode are about one order of magnitude lower than the $\widehat{v}'_{0||}$ values which show strong destabilizing effects. This may due to the small ratio of the poloidal to the parallel component of the wave vector scales that $k_{||} \sim k_\phi \ll k_\theta$ for the modes studied here in tokamak geometry.

The normalized mode growth rate γ/ω_{*e} (a) and real frequency ω/ω_{*e} (b) versus $\widehat{v}'_E$ are given for $\widehat{v}'_{0||} = 0.0,\ 0.5,$ and 1.0 in Fig. 5. For $\epsilon_n = 0.2$ the perpendicular sheared flow

always stabilizes the mode and such stabilization is almost independent of $v'_{0||}$ and the sign of v'_E. However, for slab geometry ($\epsilon_n = 0.0$) and $v_{0||} > 0$ (the solid line in Fig. 5(a)), v'_E is destabilizing first then stabilizing when it increases from zero to positive values while it is always stabilizing for negative values. This result is in agreement with that obtained under the long wavelength approximation.[12,13] The mode growth rate for $\epsilon_n = 0.2$ is twice that for $\epsilon_n = 0$ when $v'_E = 0$. However, the $\widehat{v}'_E$ values required to completely stabilize the mode for the former are almost the same as that for the later when $v'_E < 0$ and even smaller for $v'_E > 0$. This means that the stabilization effects from the perpendicular flow shear on the η_i-mode are stronger in the toroidal geometry than that in the slab.

The stabilizing effects of perpendicular shear flow on the η_i-mode is significant but the mode real frequency does not change very much with such flow. The mode real frequency changes rapidly with $\widehat{v}'_E$ only when there are parallel flow shears coexisting with the perpendicular flow shear as shown in Fig. 5(b).

The threshold η_i changing with $\widehat{v}'_E$ can be found in Fig. 6 for $k_\theta \rho_i = 0.75$, $L_n/L_s = 0.1$, $\epsilon_n = 0.2$, $\tau_e = 1$ and $\widehat{v}'_{0||} = 0.5$. The threshold value of η_i increases from $\eta_{i,\mathrm{crit}} \sim 2/3 \sim 0.7$ for $\widehat{v}'_E = 0$ to ~ 1.8 for $\widehat{v}'_E = 0.08$. At the same time, the mode growth rate for $\widehat{v}'_E = 0.08$ is about an order of magnitude smaller than that for $\widehat{v}'_E = 0.0$ when $\eta_i = 2.0$.

C. Magnetic Shear Effects

The magnetic shear parameter $\widehat{s}(r) = rdq/qdr$ in a tokamak plasma is usually small at the center and has the maximum value at the boundary. Experimentally observed perpendicular flow shear exists only in a narrow region of plasma minor radius and is typically most important in the L to H transition. A natural question to ask is where this shear flow layer should be located in order to get the maximum benefit. In other words, where the location of the sheared flow is when the confinement improvement is observed if the suppression of η_i turbulence is responsible for the improvement in the confinement.

The mode growth rate versus magnetic shear $L_n/L_s = \epsilon_n \hat{s}/q$ is given in Fig. 7 for $\hat{v}'_{0||} =$ 0, 1 and $\hat{v}'_E = 0,\ 0.05$. Comparison of the solid line ($\hat{v}'_{0||} = \hat{v}'_E = 0$) and the short dashed line ($\hat{v}'_{0||} = 1.0$, $\hat{v}'_E = 0.0$) shows that the destabilizing effect of $\hat{v}'_{0||}$ becomes slightly stronger with increasing magnetic shear for $v'_E = 0$. The destabilizing effect of $\hat{v}'_{0||} = 1$ ($dv_{0||}/dx = v_{ti}/L_n$) is overcome by the stabilization effect of $\hat{v}'_E = 0.05$ ($|dv_E/dx| = v_{ti}/20L_n$) when $L_n/L_s \lesssim 0.1$ (see the dashed line and the dot-dash line) while the destabilizing effect increases with the magnetic shear and even enhanced by the perpendicular flow shear when $L_n/L_s \gtrsim 0.3$ (see the short dashed line and the dot-dash line) for $\hat{v}'_E = 0.05$.

The curves of $\hat{v}'_{0||} = 0.0$, $\hat{v}'_E = 0.0$ (the solid line) and $\hat{v}'_{0||} = 0$, $\hat{v}'_E = 0.05$ (the dashed line) show that v'_E stabilization effect is very strong in low shear region ($L_n/L_s \lesssim 0.05$). For $L_n/L_s > 0.1$ the effectiveness of the v'_E stabilization decreases with the increase of magnetic shear. For the parameters used here the stabilization effect on the mode from $\hat{v}'_E = 0.05$ is almost negligible when $L_n/L_s \gtrsim 0.3$, although the perpendicular flow shear seems always stabilizing in the absence of parallel flow shear (see the solid line and the dashed line). For high magnetic shear, much higher $\hat{v}'_E$ is needed to suppress the η_i-mode even without the parallel sheared flow. The high effectiveness of the $v'_E(r)$ stabilization at low magnetic shear suggests that even in a shearless configuration the turbulence can be suppressed by flow shear as a substitute for the magnetic shear.

The perpendicular flow shear $\hat{v}'_E = 0.05$ can be either stabilizing or destabilizing depending on the value of the magnetic shear if there is parallel flow shear present. For $\hat{v}'_{0||} = 1$ and $\hat{v}'_E = 0.05$ (dot-dash line) perpendicular flow shear stabilization effect dominates in weak shear region ($L_n/L_s \lesssim 0.1$) compared with the solid line. Such stabilization effect is even enhanced by the presence of the parallel flow shear $\hat{v}'_{0||}$ in the region $L_n/L_s \lesssim 0.05$, compared with the dashed line ($\hat{v}'_{0||} = 0$ and $\hat{v}'_E = 0.05$). Comparison of the short dashed line ($\hat{v}'_{0||} = 1$ and $\hat{v}'_E = 0$) and the dot-dash line ($\hat{v}'_{0||} = 1$ and $\hat{v}'_E = 0.05$) shows that $\hat{v}'_E = 0.05$ is stabilizing for $L_n/L_s \lesssim 0.25$ while it is destabilizing for $L_n/L_s \gtrsim 0.3$ when $\hat{v}'_{0||} = 1$. This is in line with

the idea that edge turbulence may be caused by parallel flow shear of plasma in tokamaks.[16]

The magnetic shear effects are more clearly shown in Fig. 8 where the mode growth rate γ/ω_{*e} versus $\widehat{v}'_E$ are given for $L_n/L_s = 0.2$, 0.3, 0.4 and $\widehat{v}'_{0||} = 1$. It is easy to notice that v'_E is always stabilizing for $\widehat{v}'_E < 0$ just like that in Fig. 5 where $L_n/L_s = 0.1$. The perpendicular flow shear v'_E is, however, first destabilizing then stabilizing for $\widehat{v}'_E > 0$ as $\widehat{v}'_E$ increases. The higher the magnetic shear, the larger the destabilization region of the $\widehat{v}'_E$ value and the weaker the $\widehat{v}'_E$ stabilization effect. Shown also in Fig. 8 is the mode growth rate for $L_n/L_s = 0.3$, $\widehat{v}'_{0||} = 0$ (the solid line). The perpendicular flow shear v'_E is always stabilizing regardless of the sign of v'_E. Compared with Fig. 5(a) it is again clearly indicated that the destabilization effects of the parallel flow shear increase with the magnetic shear, especially when the perpendicular flow shear is small $|\widehat{v}'_E| \lesssim 0.1$.

D. Transport Estimate

We use the mixing length rule for transport based on the mode width Δx and the linear growth rate to relate the results obtained in this work to some observations in tokamak experiments. The η_i-mode induced transport is estimated with quasilinear theory,

$$\chi_i = \gamma(\Delta x)^2$$

where γ is the growth rate of the mode and Δx is the mode width taking to be the half-width (i.e. at the half maximum) of the real part of the eigenfunction in this work. In the units used for γ and Δx the dimensional scaling of χ_i is $\omega_{*e}\rho_i^2$.

Normalized χ_i variation with parallel and perpendicular sheared flows are shown in Figs. 9 and 10, respectively. The increase of the transport with the parallel flow shear mainly comes from the increase of the mode growth rate γ because the mode width does not change very much with such flow. Roughly speaking $\widehat{v}'_{0||} \sim 1$ ($v'_{0||} \sim v_{ti}/L_n$) is needed in order to have noticeable effects on the η_i-mode induced transport.

For the perpendicular flow shear the decrease of the η_i-mode induced transport is due not only to the decrease of the mode growth rate but also to the decrease of the mode width. Some typical eigenfunctions are given in Fig. 11 where the real part of the electrostatic potential, the eigenfunction, is plotted for $\widehat{v}'_E = 0,\ 0.04$, and 0.08. Besides shifting away from the mode rational surface $x = 0$ and becoming asymmetric about it, the eigenfunction shrinks (the half-width decreases approximately as $\Delta x \simeq \Delta_0(1 - \alpha_d|\widehat{v}'_E|)$ with $\alpha_d \simeq 7$ and the mode growth rate decreases as $\gamma = \gamma_0 \exp(-\beta_d \widehat{v}'^2_E)$ with $\beta_d \simeq 200$ for $v'_{0||} = 0$) when $|v'_E|$ increases. The eigenfunction shifts to $x > 0$ direction for $\widehat{v}'_E > 0$ and to $x < 0$ for $\widehat{v}'_E < 0$ while its shrinkage is approximately independent of the sign of the flow shear. Such shrinking of the eigenfunction is an essential feature in the reduction of the η_i-mode induced thermal transport by the perpendicular sheared flow. From Fig. 10 it is seen that in order to decrease the mixing length measure of the η_i-mode induced ion transport by a factor of 2 from the value when $v'_E = 0$, the small perpendicular flow shear value of $\widehat{v}'_E \sim 0.03$ is needed assuming that $\widehat{v}'_{0||}$ is less than 0.4 ($v'_{0||} < 0.4 v_{ti}/L_n$) and $L_n/L_s = 0.1$ with the other parameters given in the figure caption.

Hamaguchi and Horton[12] performed a three-dimensional nonlinear fluid simulation in a sheared slab geometry and showed that the anomalous ion thermal diffusivity is reduced significantly if the poloidal flow shear is sufficiently strong. The results obtained in this work are qualitatively in agreement with those of the simulations. Quantitatively speaking, the poloidal flow shear needed to reduce the ITG turbulence induced transport by a factor of two ($\chi_i \to \chi_i/2$) as given by $L_n v'_E/c_s \simeq 0.2$ in Fig. 7 of Ref. 12 appears to be about five times the shear value $L_n v'_E/v_{ti} \simeq 0.04$ given in Fig. 10 of this work for the same magnetic shear $L_n/L_s = 0.1$ and $v'_{0||} = 0$. Of course, some difference may be due to the nonlinear vortex turbulence in Ref. 12 as compared with the mixing length formula used here. The nonlinear vortex may be a self-organized state less susceptible to sheared flow stabilization.[19] Another possibility is that the flow shear stabilization effect is stronger in toroidal geometry than it

is in a sheared slab as pointed out in Sec. IVB. A complementary nonlinear picture of the effect of sheared flow is given in the work of Biglari *et al.*[20] in terms of correlation functions.

In terms of possible correlation with the confinement improvement experiment we point out that Burrell *et al.*[21] report that the radial correlation length of the fluctuation decreases when the plasma goes from L-mode to H-mode on DIII-D tokamak. Similar results are observed on CCT tokamak.[10] Assuming that the nonlinear effects only determine the amplitudes of the saturated fluctuations and that wavelengths of the saturated fluctuations are close to that of the linear eigenfunctions (no appreciable cascade nor inverse cascade occurs), then the shrinking feature of the eigenfunction presented in Fig. 11 is in good agreement with the experimental observations.

V. Discussion and Conclusions

Although we do not attempt to claim that ITG mode turbulence stabilization is responsible for H-mode confinement of tokamak plasmas in this work, it is interesting to explore the relevance of the results presented to experimental observations. A natural way for exploring the role of sheared flow in the edge confinement is to study the consequences of the parametric dependence presented here by taking the hypothesis that the η_i-mode controls the edge transport.

While the shear flow boundary layer was first reported by Ritz *et al.*[23] in the TEXT tokamak, the shear flow boundary layer studied extensively in the DIII-D tokamak provides a more natural application for the present collisionless η_i-mode based model due to the higher plasma temperature and the relatively large ion temperature gradient compared with TEXT shear flow layer. Using the Doppler shift of the C^{+4} emission line and assuming that the velocity of the carbon and deuterium thermal ion component are well coupled by collisional drag, Groebner *et al.*[22] interpret the simultaneous drop in the fluctuation level with the abrupt change of the perpendicular (and poloidal) rotation speed in the shear layer as the

evidence for the shear flow suppression of the turbulent transport. Here, we estimate the dimensionless stability parameters for the L and H mode phases of this experiment in an attempt assess the theoretical support for this interpretation of the improved confinement with respect to the ion temperature gradient form of the drift wave turbulence.

Estimates of the gradients of the temperature, the perpendicular and parallel flow velocities in the shear layer are given in Table I as derived from the data in Groebner *et al.*[22] The estimates for the magnetic shear length L_s and the density gradient scale length L_n should only be regarded as reference values since it is rather difficult to determine these parameters accurately in the shear layer. More detailed profile evaluations are given in Ref. 24 but problems still remain for determining better estimates of the values of L_s and L_n in the shear layer. Figure 3 in Ref. 22 is used to estimate the range of L_n and the value of $L_s \simeq 80\,\mathrm{cm}$ is used.[22]

Even though the estimates given here in Table II for the dimensionless stability parameters are rather rough, the values when viewed with respect to our figures, especially Figs. 1, 5(a), 9 and 10 appear to reveal certain important conclusions. It appears fairly clear that the increase of $\widehat{v}'_E$ in the L to H transition is sufficient to be a strong stabilizing effect on the turbulence. On the other hand, the change in the transport related to the values for $\widehat{v}'_{0\|}$ estimated from the C^{+4} data appears too small to have much effect on the turbulent transport.

Considering that some plasma parameters such as η_i, L_n/L_s, T_e/T_i are not from the same specific experimental observations this comparison is very rough. Detailed comparison is beyond the scope of this work and may be made when more complete experimental data sets are available. Another uncertainty enters through the assumption that the thermal ion component has the same velocity as the carbon component used to measure the flow velocities.

In summary, parallel sheared flow has a destabilizing effect on kinetic toroidal η_i-mode

while the perpendicular sheared flow is stabilizing. The mixing length transport formula shows that η_i-mode induced ion transport strongly decreases with the increase of the radial shear of the perpendicular flow $v_E(r)$. The decrease of the η_i-mode induced transport is due not only to the decrease of the mode growth rate but also to the shrinking of the eigenfunction. The parameters used in this work are reasonably close to the experimental values inferred for the shear layer in DIII-D so that the results presented in this work are expected to be related to the improvement of plasma confinement in the H-mode state of the discharges.

Although the poloidal flow shear is always positive ($v'_E(r) > 0$) in the spontaneous H mode with plasma heating,[9,22,25] the appreciable effects of a negative flow shear on the suppression of the turbulence and on the improvement of plasma confinement are confirmed by the experiments with biased limiter.[26] Thus as far as the sign of flow shear is concerned the results presented in Fig. (5a) and Sec. IVD, which show that the stabilization effect is approximately independent of the sign if the parallel flow shear is negligible, are consistent with experimental observations. (With regard to the sign of $v_E(r)$ it should be noted that the minus sign in $v_E = -E_r/B$ is dropped in some experimental publications.)

The relative effectiveness of the stabilization from the perpendicular flow shear depends on the strength of the magnetic shear. For weak magnetic shear $L_n/L_s \lesssim 0.1$ the shear flow stabilization is strong while for strong magnetic shear $L_n/L_s \gtrsim 0.3$ the shear flow stabilization is a weak effect. This result suggests that there is a trade-off in the effectiveness of shear flow versus magnetic shear as a mechanism for providing plasma confinement, and suggests that further studies on the effectiveness of weak magnetic shear and high flow shear be undertaken.

Besides the destabilization effects on the ITG driven modes the parallel flow shear can drive instability even without the ion temperature gradient if $|v'_{0\|}| \gtrsim (1-2)v_{ti}/L_n$, which can be satisfied for flat density profiles in the interior of the tokamak plasma or strong flow

shear due to unbalanced neutral beam injection heating.

Various theories have been proposed to account for the source of the flow velocities[27–29] which is not discussed in this work. The effects of particle collision are not taken into account in this work and may be important at the plasma edge for some H mode discharges. The self-consistent velocity source must be addressed in the future in order to understand the fundamental physical relation between the kinetic ITG mode and the L to H transition.

Acknowledgments

The authors are grateful to R. Groebner, General Atomics, for providing the DIII-D experimental data and helpful discussions, and also thank the Edge Physics Study Group, at the University of Texas at Austin, for the encouragement and interest in this work. This work was supported by the U.S. Department of Energy contract DE-FG05-80ET-53088.

References

1. F.X. Sölder, E.R. Müller, F. Wagner, H.S. Bosch, A. Eberhagen, H.V. Fahrbach, G. Fussmann, O. Ghre, K. Gentle, J. Gernhardt, O. Gruber, W. Herrmann, G. Janeschitz, M. Kornherr, K. Krieger, H.M. Mayer, K. McCormick, H.D. Murmann, J. Neuhauser, R. Nolte, W. Poschenreider, H. Röhr, H.-H. Steuer, U. Stroth, N. Tsois, and H. Verbeek, Phys. Rev. Lett. **61**, 1105 (1988).

2. R.J. Fonk, R. Howell, K. Jaehnig, L. Roquemore, G. Schilling, S. Scott, M.C. Zarnstorff, C. Bush, R. Goldston, H. Hsuan, D. Johnson, A. Ramsey, J. Schivell, and H. Towner, Phys. Rev. Lett. **63**, 520 (1989).

3. S.D. Scott, P.H. Diamond, R.J. Fonck, R.B. Howell, K.P. Jahnig, G. Schilling, E.J. Synakowski, M.C. Zarnstorff, C.E. Bush, E. Fredrickson, K.W. Hill, A.C. Janos, D.K. Mansfield, D.K. Owens, H. Park, G. Pautasso, A.T. Ramsey, J. Schivell, G.D. Tait, W.M. Tang, and G. Taylor, Phys. Rev. Lett. **64**, 531 (1990).

4. W. Horton, D. Lindberg, J.-Y. Kim, J.Q. Dong, G.W. Hammett, S.D. Scott, M.C. Zarnstorff, and S. Hamaguchi, Phys. Fluids B **4**, 531 (1992).

5. J.-Y. Kim and W. Horton, Phys. Fluids B **3**, 1167 (1991).

6. X.Q. Xu and M.N. Rosenbluth, Phys. Fluids B **3**, 627 (1991).

7. K.H. Burrell, *et al.*, Plasma Physics and Contr. Fusion **31**, 1649 (1989).

8. R.J. Groebner, K.H. Burrell, and R.P. Seraydarian, Phys. Rev. Lett. **64**, 3015 (1990).

9. K. Ida, *et al.*, Phys. Rev. Lett. **65**, 1364 (1990); K. Ida, *et al.*, Phys. Fluids B **4**, 2552 (1992).

10. R.J. Taylor, *et al.*, Phys. Rev. Lett. **63**, 2365 (1989).

11. HL-1 Group, P.R. China, private communication (1991).

12. S. Hamaguchi and W. Horton, Phys. Fluids B **4**, 319 (1992).

13. M. Artun and W.M. Tang, Phys. Fluids B **4**, 1102 (1992).

14. G.M. Staebler and R.R. Dominguez, Nucl. Fusion **31**, 1891 (1991).

15. P.J. Catto, M.N. Rosenbluth, and C.S. Liu, Phys. Fluids **16**, 1719 (1973).

16. P.N. Guzdar, J.F. Drake, J.M. Finn, V. Shapiro, V. Sherchenko, F. Waelbroeck, A. Hassam, C.S. Liu, and R.Z. Sagdeev, private communication.

17. J.Q. Dong, W. Horton, and J.-Y. Kim, Phys. Fluids B **4**, 1867 (1992).

18. G. Ganguli and Y.C. Lee, Phys. Fluids **31**, 823 (1988).

19. W. Horton, D. Jovanovic, and J. Juul Rasmussen, to be published in Phys. Fluids B **4**, October (1992).

20. H. Biglari, P.H. Diamond, P.W. Terry, Phys. Fluids B **2**, 1 (1990).

21. K.H. Burrell, R.J. Groebner, T.K. Kurki-Suonio, *et al.*, in Plasma Physics and Nuclear Fusion Research 1990 (Proc. 13th Int. Conf., Washington, DC, 1990), Vol. 1, IAEA (1991) 123.

22. R.J. Groebner, W.A. Peebles, K.H. Burrell, T.N. Carlstrom, P. Gohil, R.P. Seraydarian, E.J. Doyle, R. Philipona, H. Matsumato, and B. Cluggish, ibid., p. 453; R.J. Groebner, private communications.

23. Ch. P. Ritz, R.D. Bengtson, S.J. Levison, and E.J. Powers, Phys. Fluids. **27**, 2956 (1984).

24. T.K. Kurki-Suonio, R.J. Groebner, and K.H. Burrell, Nucl. Fusion **32**, 133 (1992).

25. K. ida, S. Hidekuma, and M. Kojima, Phys. Fluids B **4**, 2552 (1992).

26. R. Van Nieuwenhove, G. Van Oost, R.R. Weynants, J. Boedo, D. Bora, T. Delvigne, F. Durodie, M. Gaigneaux, D.S. Gray, B. Giesen, R.S. Ivanov, R. Leners, Y.T. Lie, A.M. Messiaen, A. Pospieszczyck, U. Samm, R.P. Schorn, B. Schweer, C. Stickelmann, G. Telesca, P.E. Vandenplas, in Proceedings of the 18th Europ. Conf. on Controlled Fusion and Plasma Phys., Vol. 15 C, Part I, 406 (1991).

27. K.C. Shaing and E.C. Crume, Jr., Phys. Rev. Lett. **63**, 2369 (1989).

28. R.D. Hazeltine, Phys. Fluids B **1**, 2031 (1989).

29. A.B. Hassam, T.M. Antonsen, Jr., J.F. Drake, and C.S. Liu, Phys. Rev. Lett. **66**, 309 (1991).

Figure Captions

1. Normalized mode growth rate $\gamma k_\theta \rho_i/\omega_{*e}$ vs. wavenumber $k_\theta \rho_i$ for $\widehat{v}'_{0||} = L_n dv_{0||}/v_{ti}dx = 0.0,\ 0.2$, and 0.5 and the fluid approximation. The other parameters are $\eta_i = 2.5$, $L_n/L_s = 0.1$, $\epsilon_n = 0.25$, $T_e/T_i = 1.0$, $\widehat{v}'_E = 0.0$.

2. Normalized mode growth rate γ/ω_{*e} vs. parallel flow shear $\widehat{v}'_{0||} = L_n dv_{||}/v_{ti}dx$ for $\epsilon_n = 0.0,\ 0.1, 0.25$ and the fluid approximation in slab ($\epsilon_n = 0$). The other parameters are $\eta_i = 2.5$, $k_\theta \rho_i = 0.5$, $L_n/L_s = 0.1$, $T_e/T_i = 1.0$, $\widehat{v}'_E = 0.0$.

3. Normalized mode growth rate γ/ω_{*e} (a) and real frequency ω/ω_{*e} (b) vs. η_i for $\widehat{v}'_{0||} = L_n dv_{||}/v_{ti}dx = 0.0,\ 0.5,\ 1.0$, and 2.0. The other parameters are $k_\theta \rho_i = 0.75$, $L_n/L_s = 0.1$, $\epsilon_n = 0.2$, $T_e/T_i = 1.0$, $\widehat{v}'_E = 0.0$.

4. Normalized mode growth rate $\gamma k_\theta \rho_i/\omega_{*e}$ vs. wavenumber $k_\theta \rho_i$ for $\widehat{v}'_E = L_n dv_e/v_{ti}dx = 0.0,\ 0.04$, and 0.08. The other parameters are $\eta_i = 2.5$, $L_n/L_s = 0.1$, $\epsilon_n = 0.25$, $T_e/T_i = 1.0$, $\widehat{v}'_{0||} = 0.5$.

5. Normalized mode growth rate (a) and real frequency ω/ω_{*e} (b) vs. perpendicular flow shear $\widehat{v}'_E = L_n dv_e/v_{ti}dx$ for $\widehat{v}'_{0||} = 0.0,\ 0.5,\ 1.0$. The other parameters are $\eta_i = 2.5$, $k_\theta \rho_i = 0.75$, $L_n/L_s = 0.1$, $\epsilon_n = 0.20$, $T_e/T_i = 1.0$. The solid line is for slab $\epsilon_n = 0$, $\widehat{v}'_{0||} = 1$ and the other parameters are the same as above.

6. Normalized mode growth rate γ/ω_{*e} vs. η_i for $\widehat{v}'_E = 0.0,\ 0.04,\ 0.08$. The other parameters are $k_\theta \rho_i = 0.75$, $L_n/L_s = 0.1$, $\epsilon_n = 0.2$, $T_e/T_i = 1.0$, $\widehat{v}'_{0||} = 0.5$.

7. Normalized mode growth rate γ/ω_{*e} vs. the magnetic shear L_n/L_s for different $\widehat{v}'_{0||}$ and $\widehat{v}'_E$. The other parameters are $\eta_i = 2.5$, $\epsilon_n = 0.2$, $T_e/T_i = 1.0$, $\rho_i = 0.75$.

8. Normalized mode growth rate γ/ω_{*e} vs. perpendicular flow shear $\widehat{v}'_E = L_n dv_e/v_{ti}dx$ for $L_n/L_s = 0.2,\ 0.3,\ 0.4$. The other parameters are $\eta_i = 2.5$, $k_\theta \rho_i = 0.75$, $\widehat{v}_{0||} = 1.0$, $\epsilon_n = 0.20$, $T_e/T_i = 1.0$.

9. Quasilinear thermal transport $\gamma(\Delta x)^2/\rho_i^2\omega_{*e}$ vs. $\widehat{v}'_{0||} = L_n dv_{0||}/v_{ti}dx$ for $\epsilon_n = 0.0,\ 0.1,\ 0.25$. The other parameters are $\eta_i = 2.5$, $k_\theta \rho_i = 0.5$, $L_n/L_s = 0.1$, $T_e/T_i = 1.0$, $\widehat{v}'_E = 0.0$.

10. Quasilinear thermal transport $\gamma(\Delta x)^2/\rho_i^2\omega_{*e}$ vs. $\widehat{v}'_E = L_n dv_E/v_{ti}dx$ for $\widehat{v}'_{0||} = 0.0,\ 0.5,\ 1.0$. The other parameters are $\eta_i = 2.5$, $k_\theta \rho_i = 0.75$, $L_n/L_s = 0.1$, $T_e/T_i = 1.0$, $\epsilon_n = 0.2$.

11. The real part of the eigenfunction $\phi_r(x/\rho_i)$ for $\widehat{v}'_E = 0.0,\ 0.04,\ 0.08$. The other parameters are $\eta_i = 2.5$, $k_\theta \rho_i = 0.5$, $L_n/L_s = 0.1$, $T_e/T_i = 1.0$, $\widehat{v}'_{0||} = 0.0$.

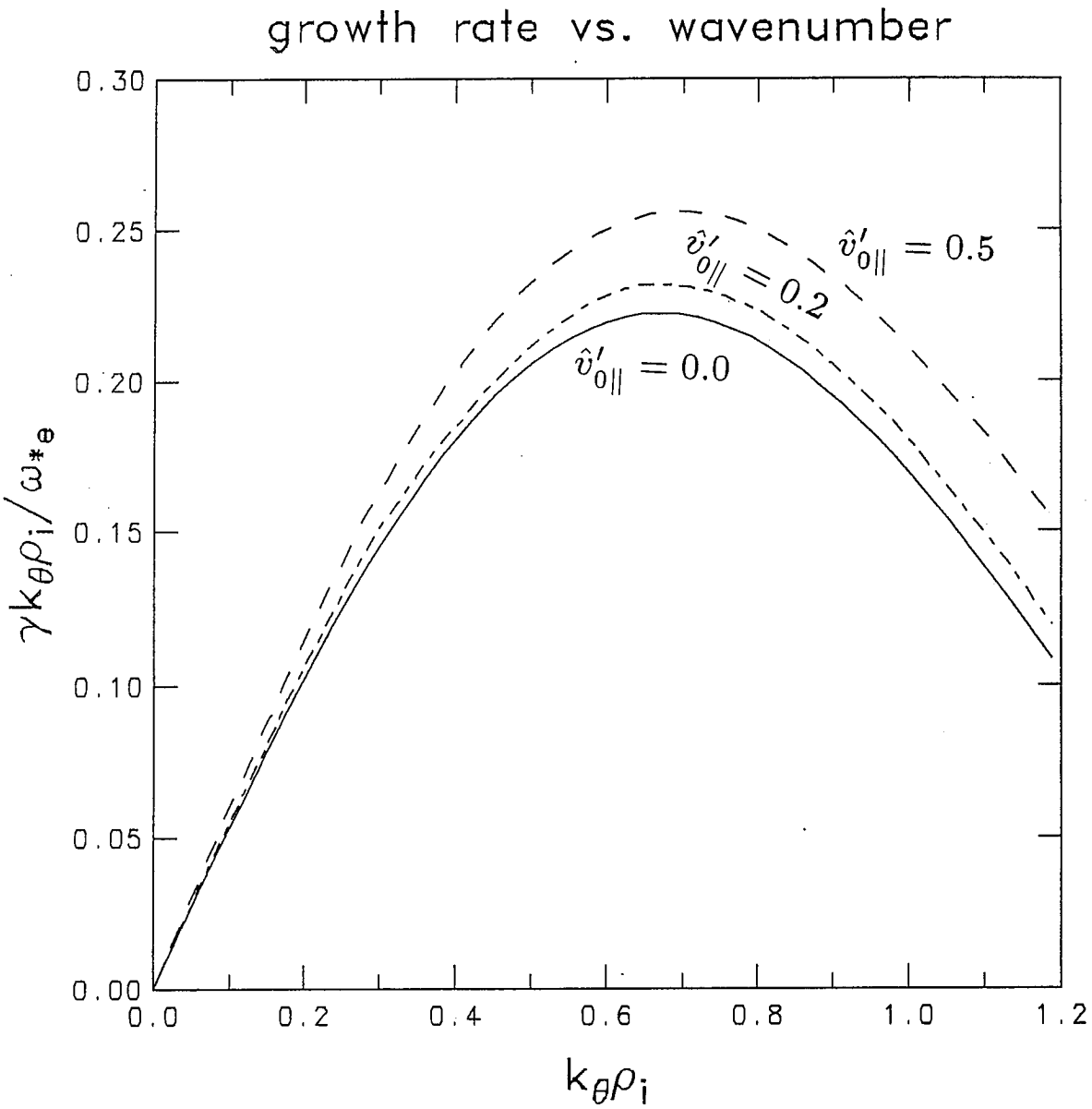
growth rate vs. wavenumber
0.30
0.25
0.20
0.15
0.10
0.05
0.00
0.0
0.2
0.4
0.6
0.8
1.0
1.2
$\gamma k_\theta \rho_i / \omega_{*e}$
$k_\theta \rho_i$
$\hat{v}'_{0\|} = 0.5$
$\hat{v}'_{0\|} = 0.2$
$\hat{v}'_{0\|} = 0.0$

Fig. 1

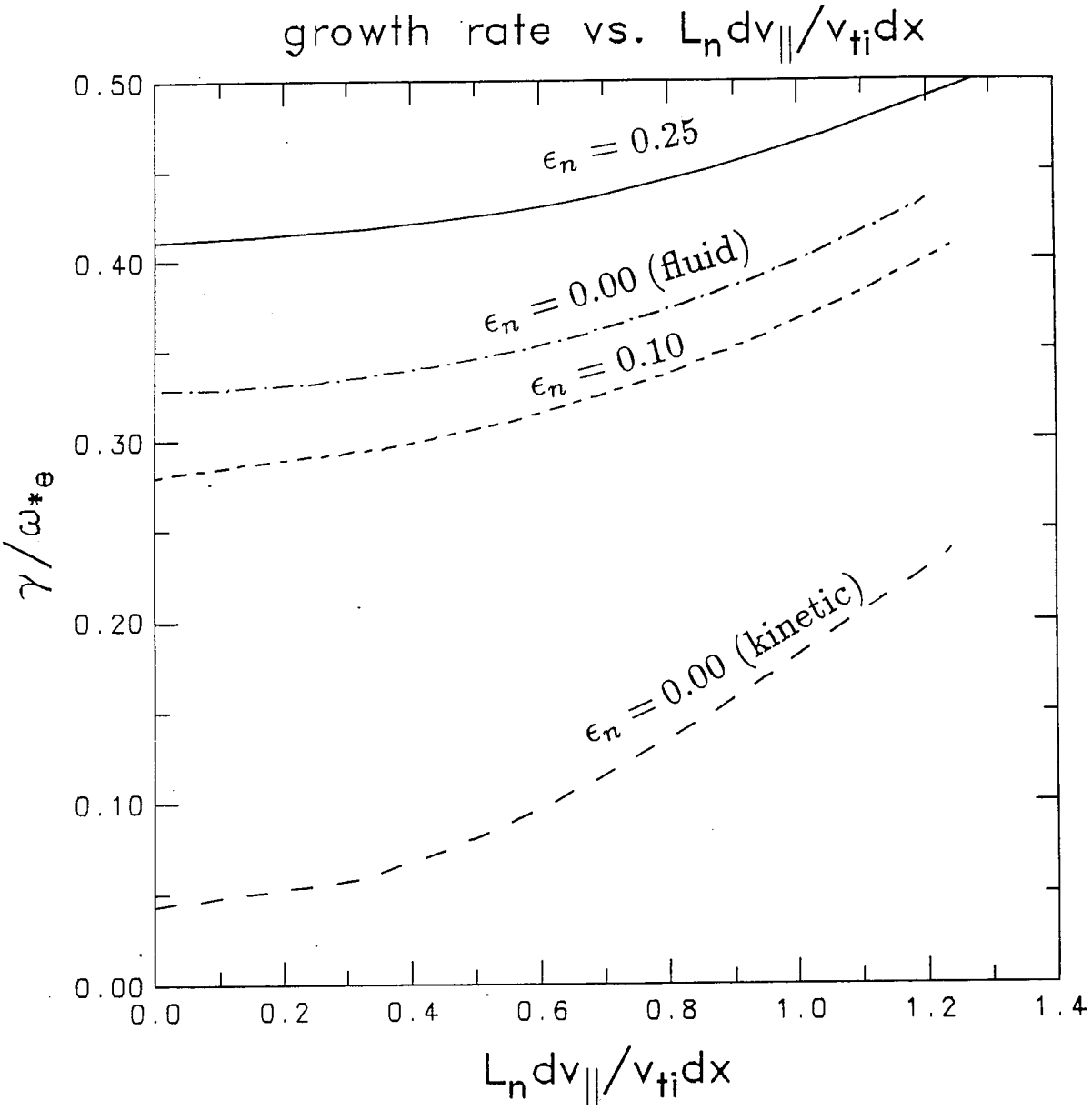
growth rate vs. $L_n dv_{||}/v_{ti} dx$
0.50
0.40
0.30
0.20
0.10
0.00
0.0
0.2
0.4
0.6
0.8
1.0
1.2
1.4
γ/ω_{*e}
$L_n dv_{||}/v_{ti} dx$
$\epsilon_n = 0.25$
$\epsilon_n = 0.00$ (fluid)
$\epsilon_n = 0.10$
$\epsilon_n = 0.00$ (kinetic)

Fig. 2

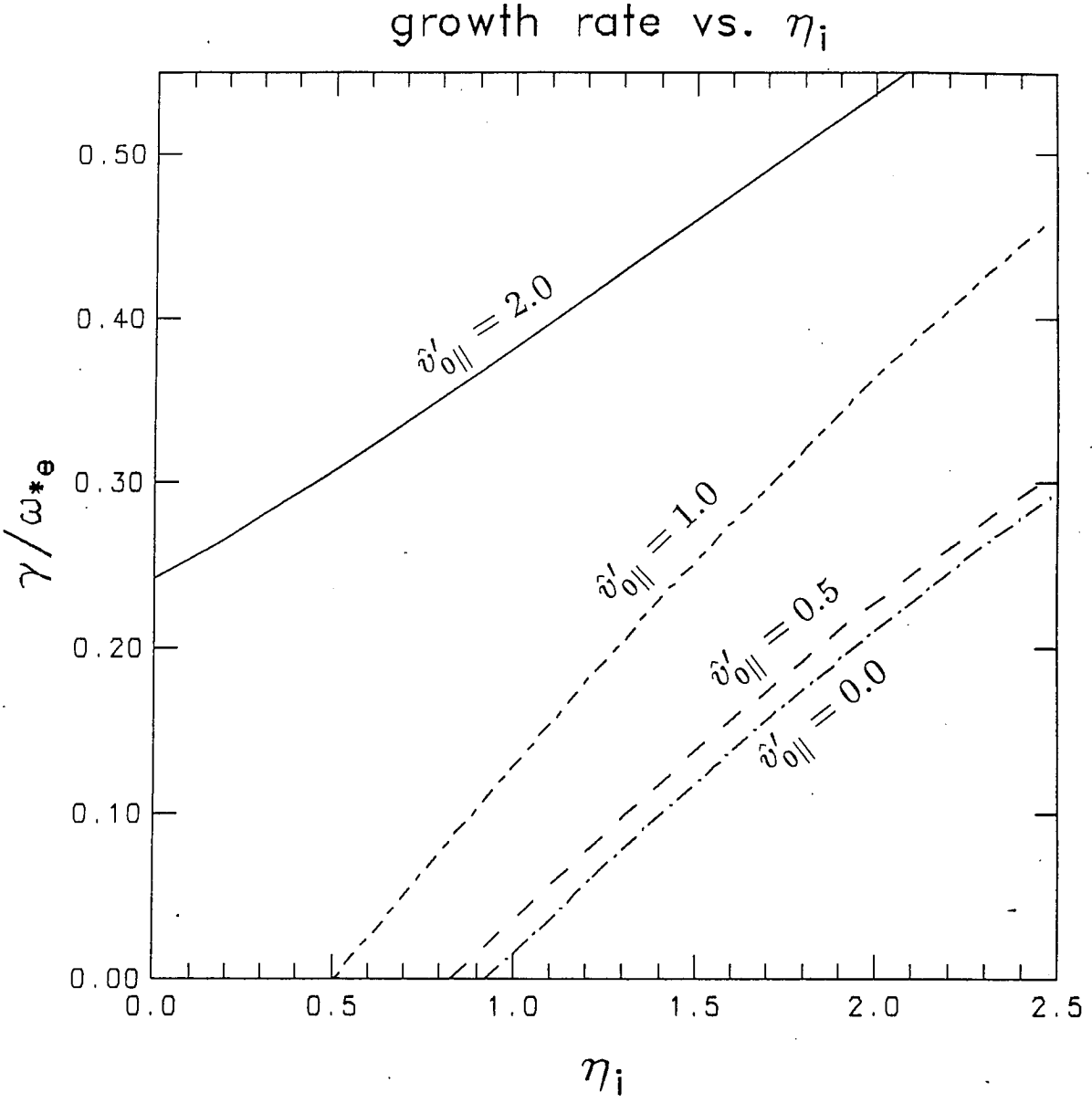
growth rate vs. η_i
0.50
0.40
0.30
0.20
0.10
0.00
γ / ω_{*e}
$\hat{v}'_{0\|} = 2.0$
$\hat{v}'_{0\|} = 1.0$
$\hat{v}'_{0\|} = 0.5$
$\hat{v}'_{0\|} = 0.0$
0.0
0.5
1.0
1.5
2.0
2.5
η_i

Fig. 3a

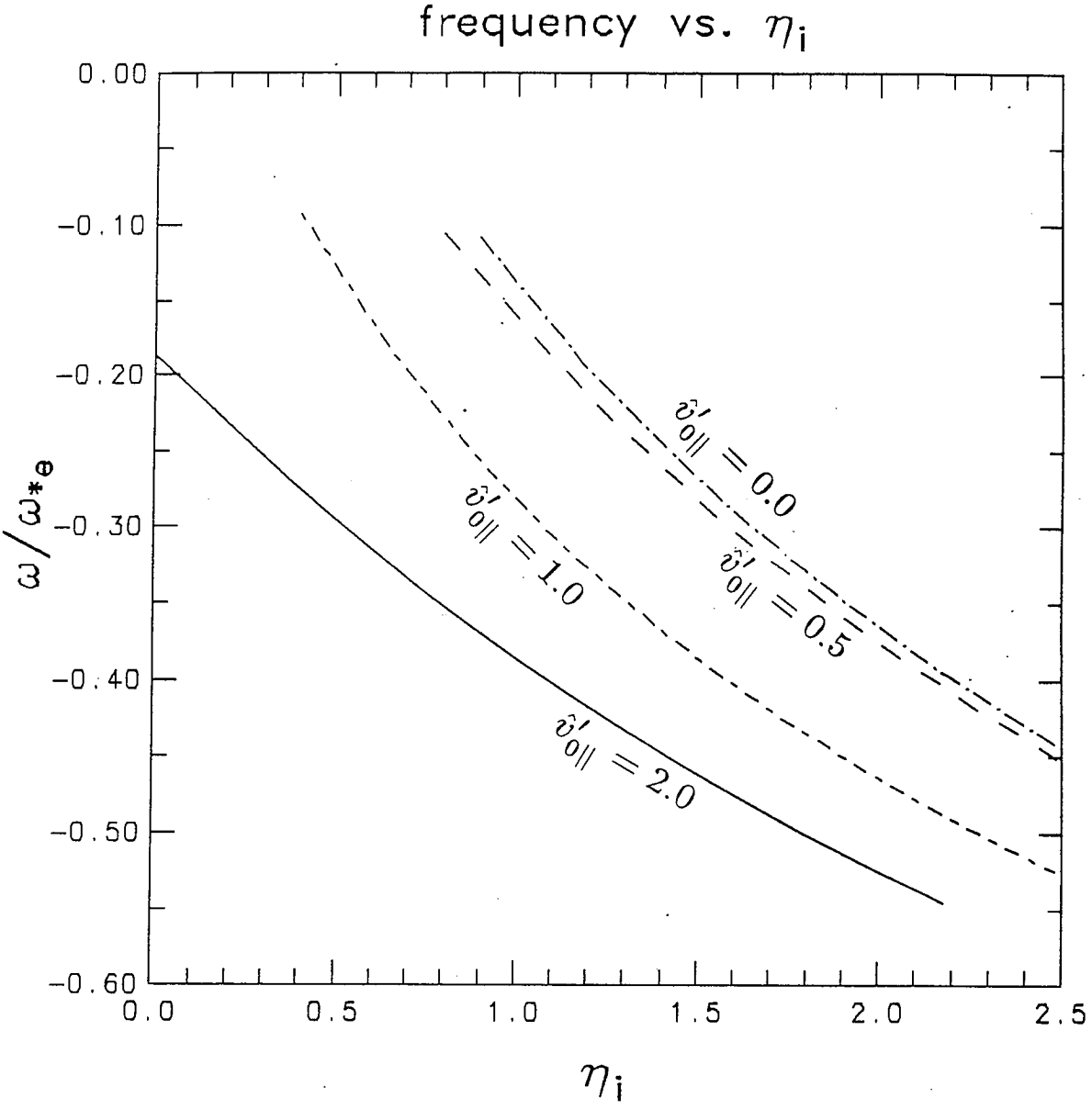
frequency vs. η_i
0.00
-0.10
-0.20
-0.30
-0.40
-0.50
-0.60
ω/ω_{*e}
0.0
0.5
1.0
1.5
2.0
2.5
η_i
$\hat{v}'_{o\|} = 0.0$
$\hat{v}'_{o\|} = 0.5$
$\hat{v}'_{o\|} = 1.0$
$\hat{v}'_{o\|} = 2.0$

Fig. 3b

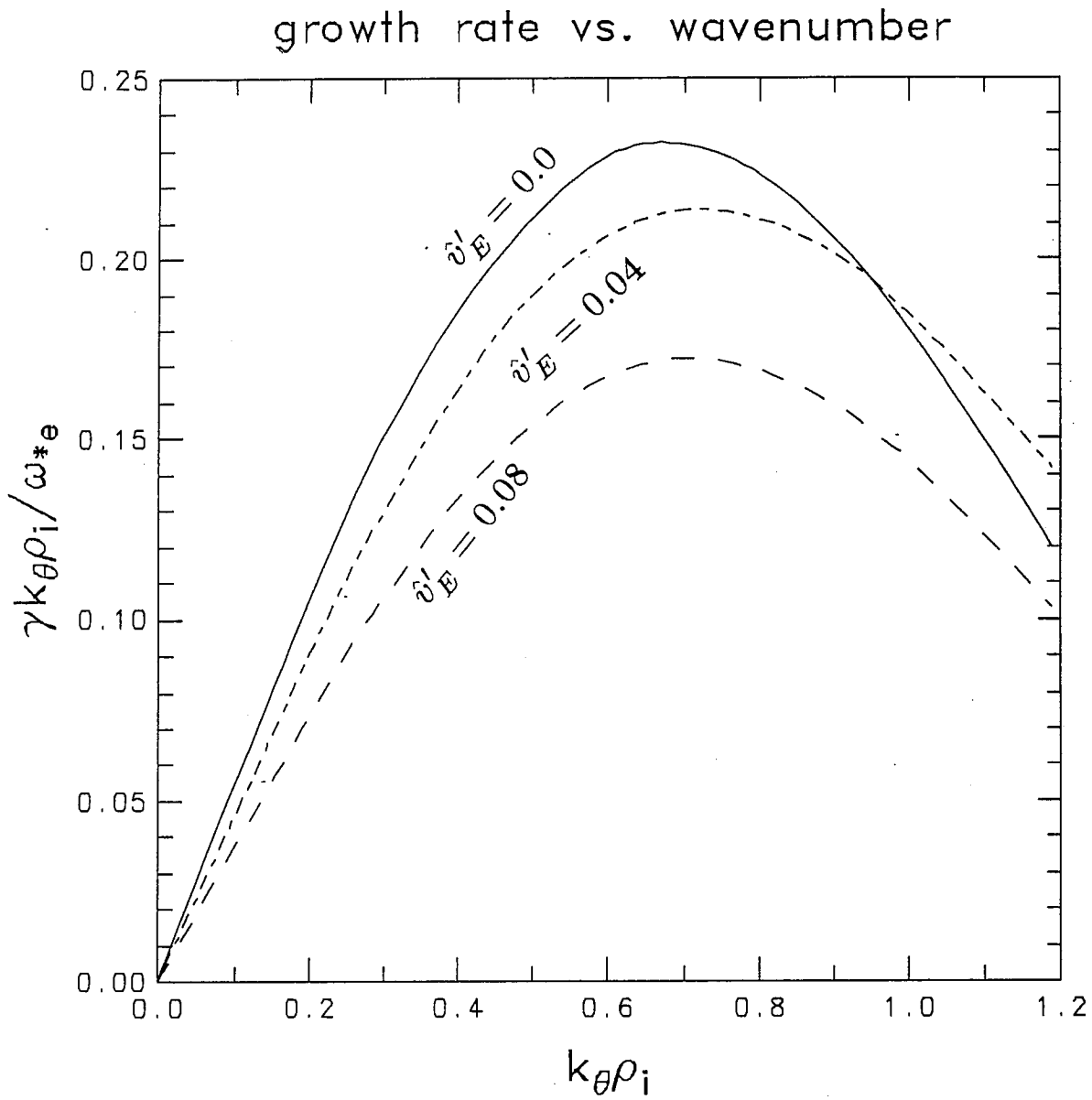
growth rate vs. wavenumber
0.25
0.20
0.15
0.10
0.05
0.00
0.0
0.2
0.4
0.6
0.8
1.0
1.2
$\gamma k_\theta \rho_i / \omega_{*e}$
$k_\theta \rho_i$
$\hat{v}'_E = 0.0$
$\hat{v}'_E = 0.04$
$\hat{v}'_E = 0.08$

Fig. 4

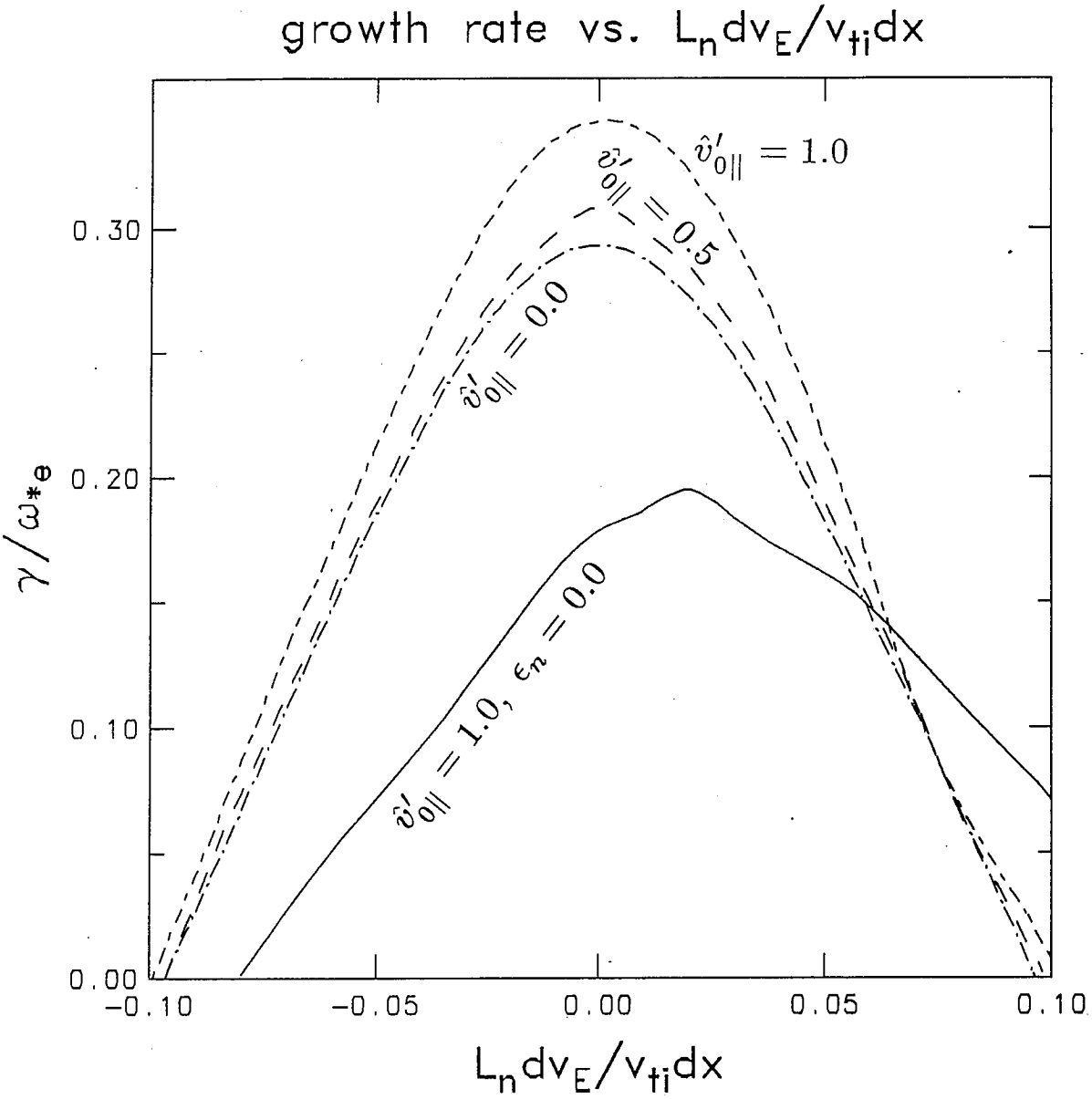
growth rate vs. $L_n dv_E/v_{ti}dx$
$\hat{v}'_{0\|} = 1.0$
$\hat{v}'_{0\|} = 0.5$
$\hat{v}'_{0\|} = 0.0$
$\hat{v}'_{0\|} = 1.0,\ \epsilon_n = 0.0$
γ/ω_{*e}
0.00
0.10
0.20
0.30
−0.10
−0.05
0.00
0.05
0.10
$L_n dv_E/v_{ti}dx$

Fig. 5a

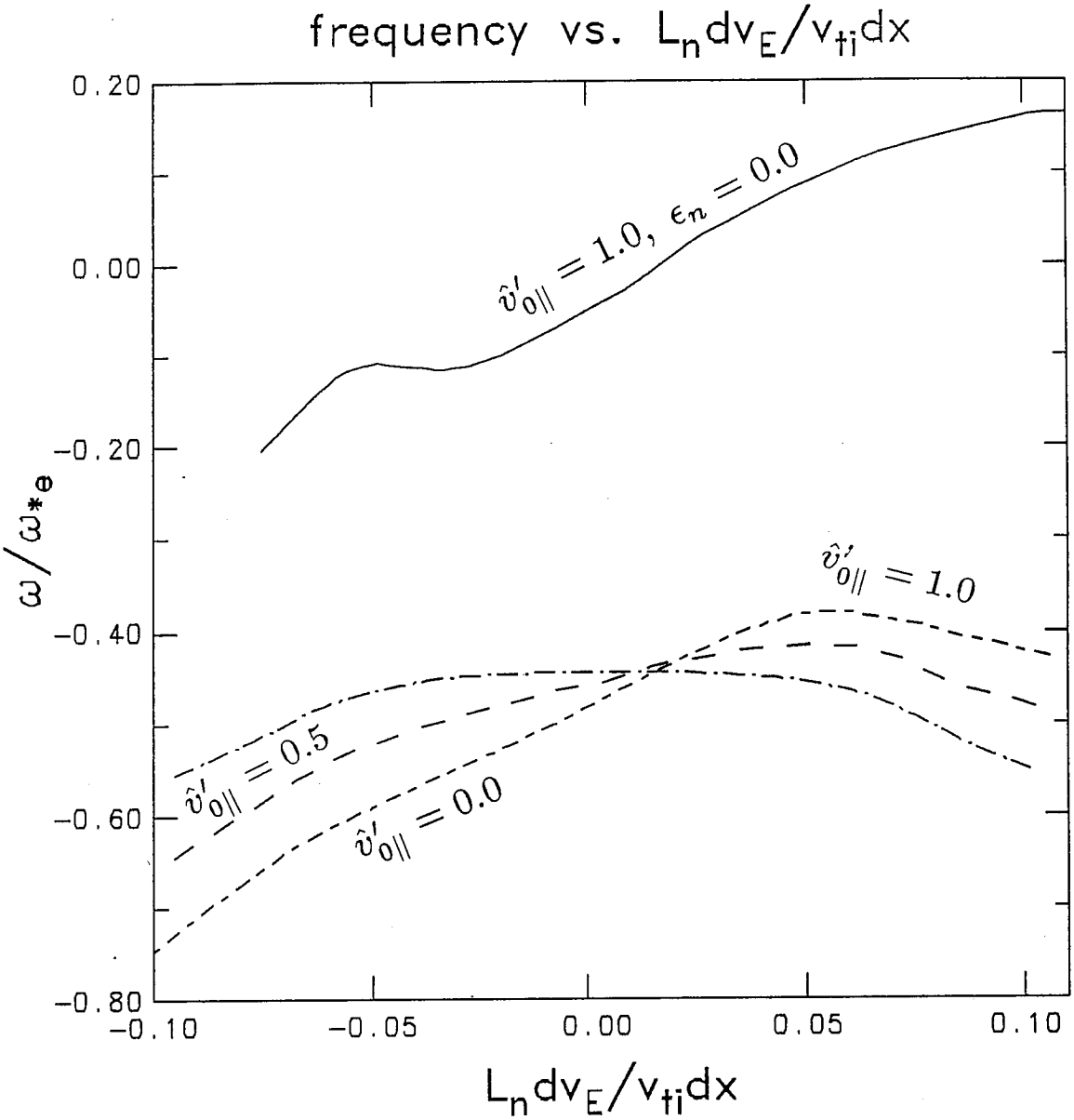
frequency vs. $L_n dv_E/v_{ti}dx$
0.20
0.00
−0.20
−0.40
−0.60
−0.80
ω/ω_{*e}
−0.10
−0.05
0.00
0.05
0.10
$L_n dv_E/v_{ti}dx$
$\hat{v}'_{0\|} = 1.0,\ \epsilon_n = 0.0$
$\hat{v}'_{0\|} = 1.0$
$\hat{v}'_{0\|} = 0.5$
$\hat{v}'_{0\|} = 0.0$

Fig. 5b

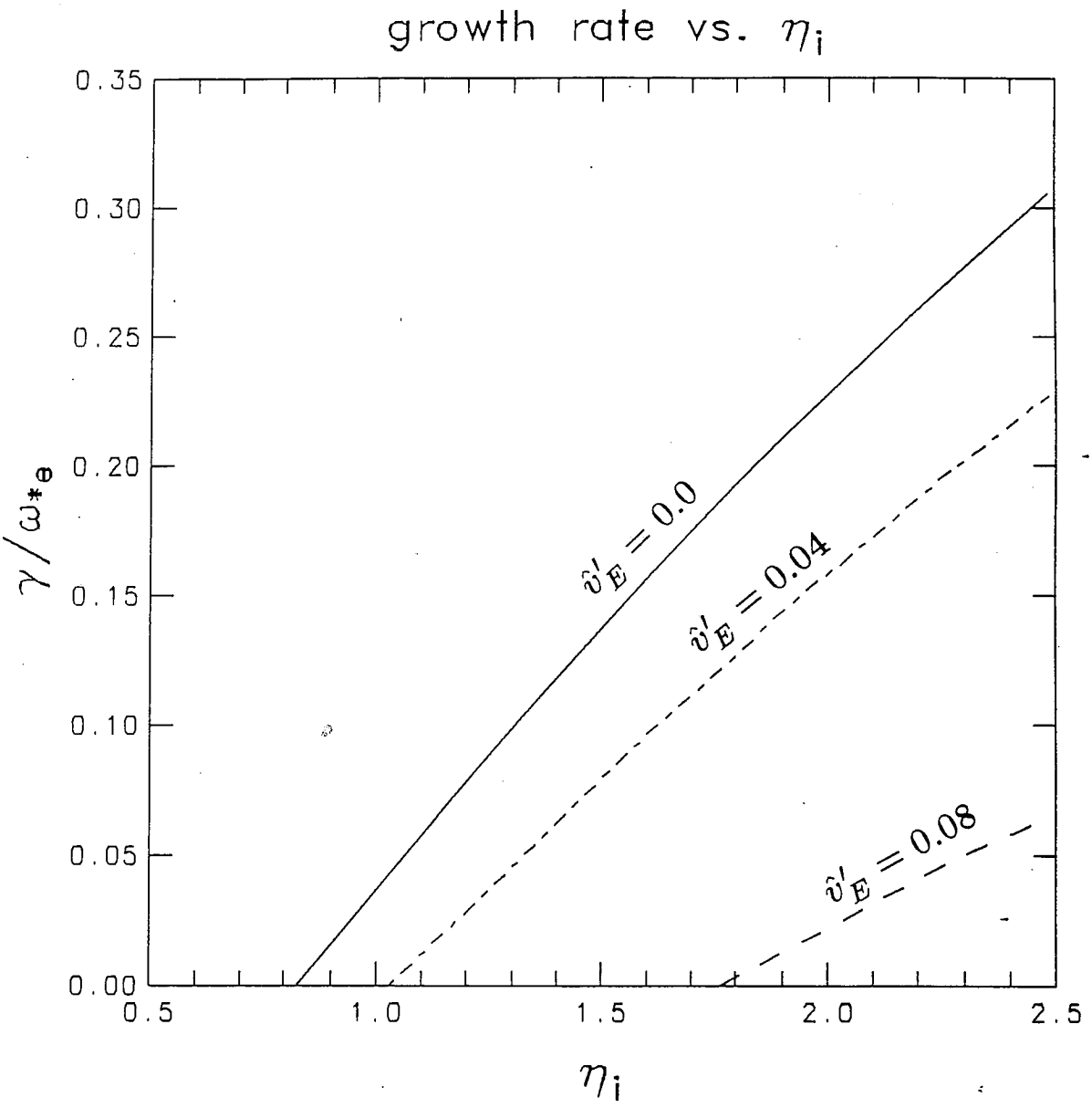
growth rate vs. η_i
0.35
0.30
0.25
0.20
0.15
0.10
0.05
0.00
γ/ω_{*e}
0.5
1.0
1.5
2.0
2.5
η_i
$\hat{v}'_E = 0.0$
$\hat{v}'_E = 0.04$
$\hat{v}'_E = 0.08$

Fig. 6

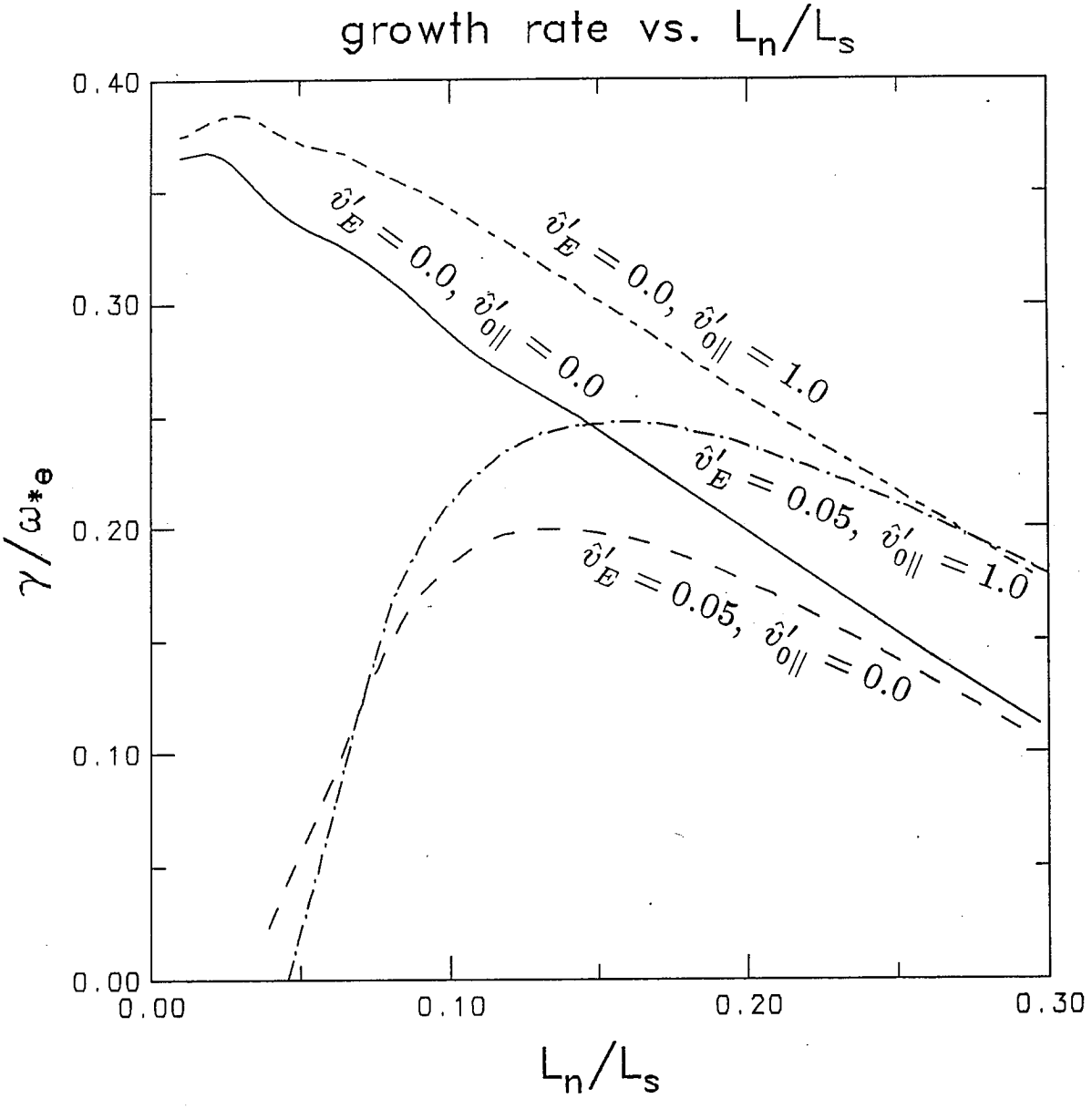
growth rate vs. L_n/L_s
0.40
0.30
0.20
0.10
0.00
0.00
0.10
0.20
0.30
γ/ω_{*e}
L_n/L_s
$\hat{v}'_E = 0.0,\ \hat{v}'_{0\|} = 1.0$
$\hat{v}'_E = 0.0,\ \hat{v}'_{0\|} = 0.0$
$\hat{v}'_E = 0.05,\ \hat{v}'_{0\|} = 1.0$
$\hat{v}'_E = 0.05,\ \hat{v}'_{0\|} = 0.0$

Fig. 7

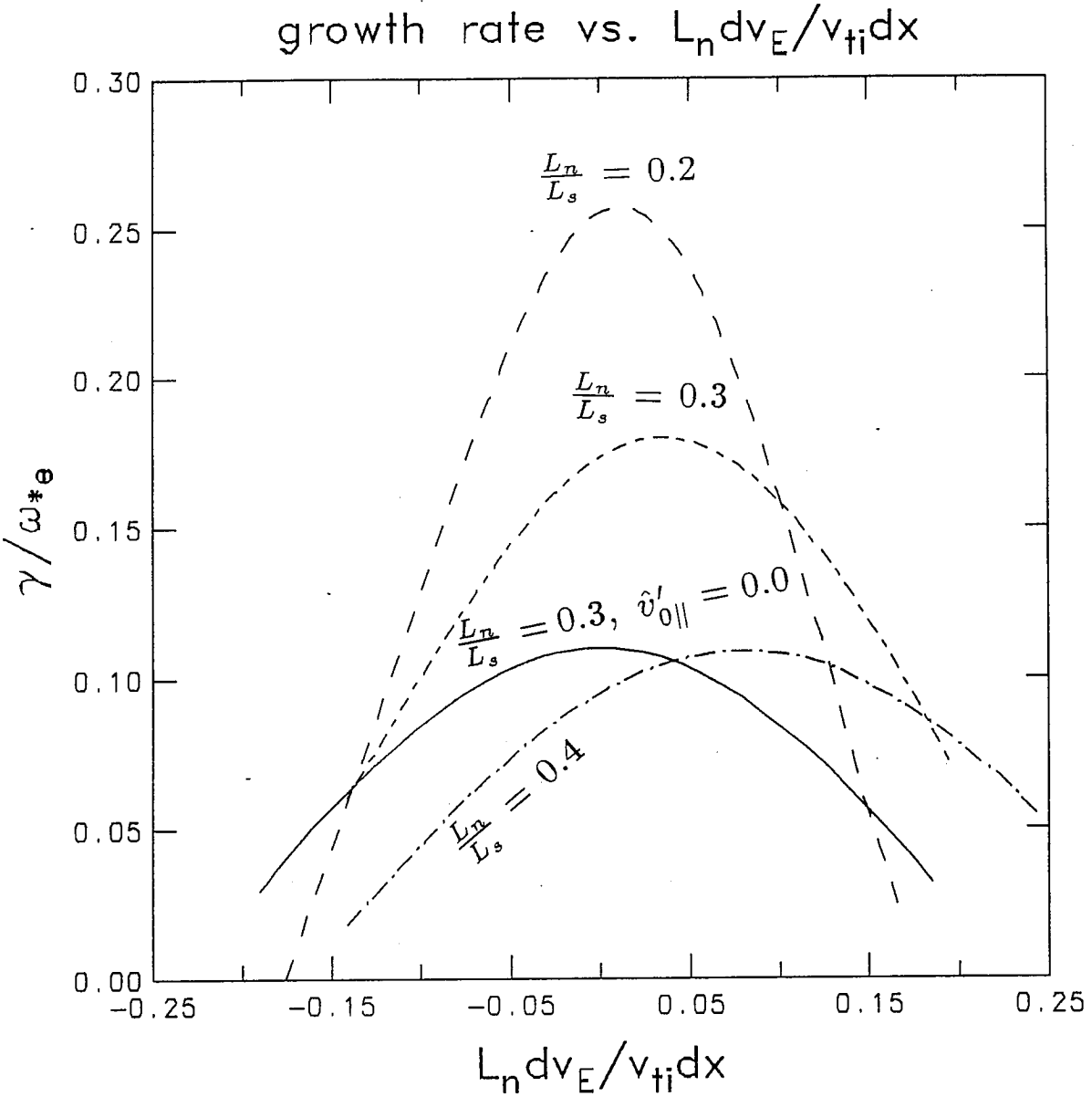
growth rate vs. $L_n dv_E/v_{ti} dx$
0.30
0.25
0.20
0.15
0.10
0.05
0.00
γ/ω_{*e}
$\frac{L_n}{L_s} = 0.2$
$\frac{L_n}{L_s} = 0.3$
$\frac{L_n}{L_s} = 0.3,\ \hat{v}'_{0\|} = 0.0$
$\frac{L_n}{L_s} = 0.4$
−0.25
−0.15
−0.05
0.05
0.15
0.25
$L_n dv_E/v_{ti} dx$

Fig. 8

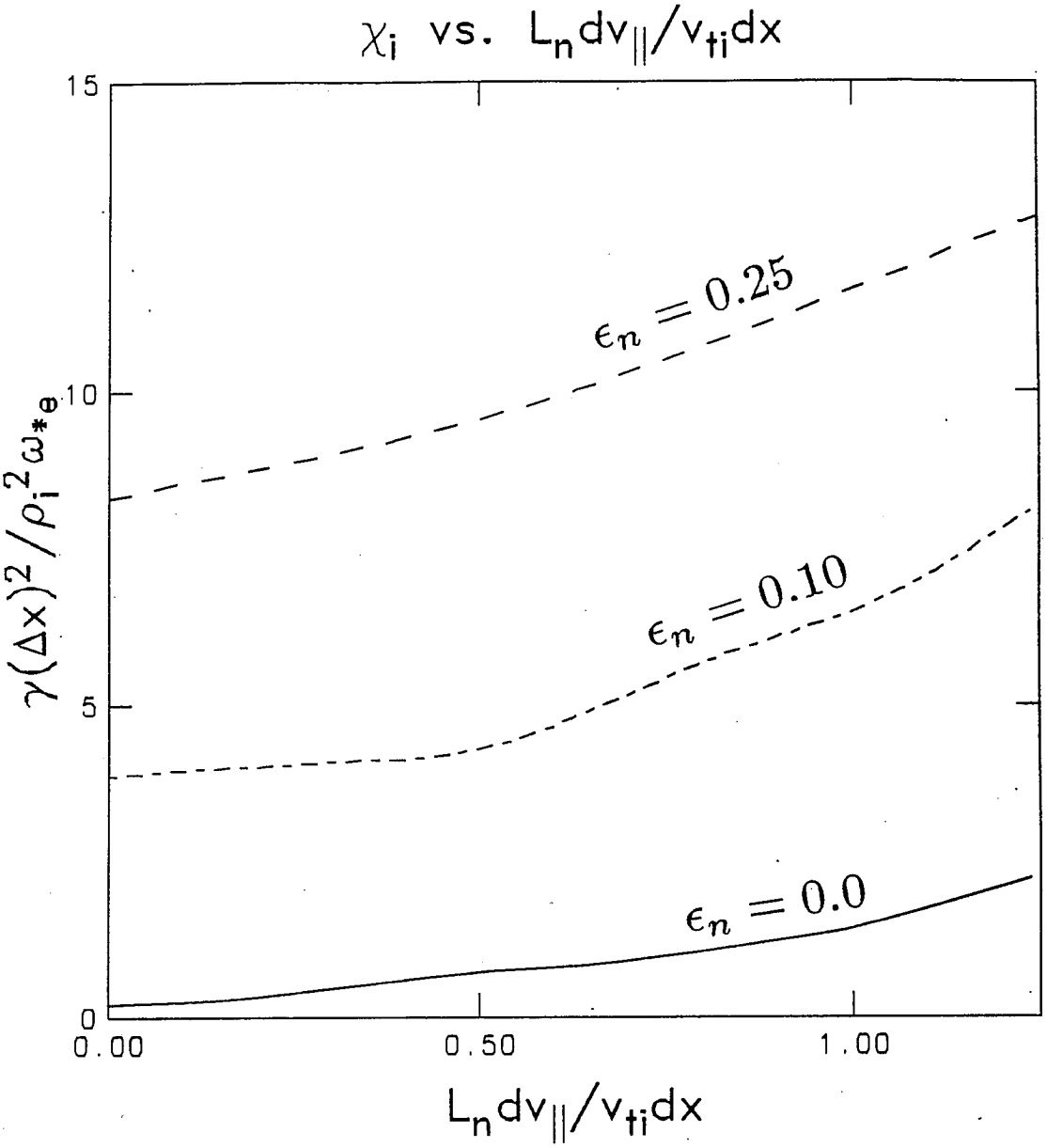
χ_i vs. $L_n dv_{||}/v_{ti}dx$
15
10
5
0
0.00
0.50
1.00
$\gamma(\Delta x)^2/\rho_i^2\omega_{*e}$
$\epsilon_n = 0.25$
$\epsilon_n = 0.10$
$\epsilon_n = 0.0$
$L_n dv_{||}/v_{ti}dx$

Fig. 9

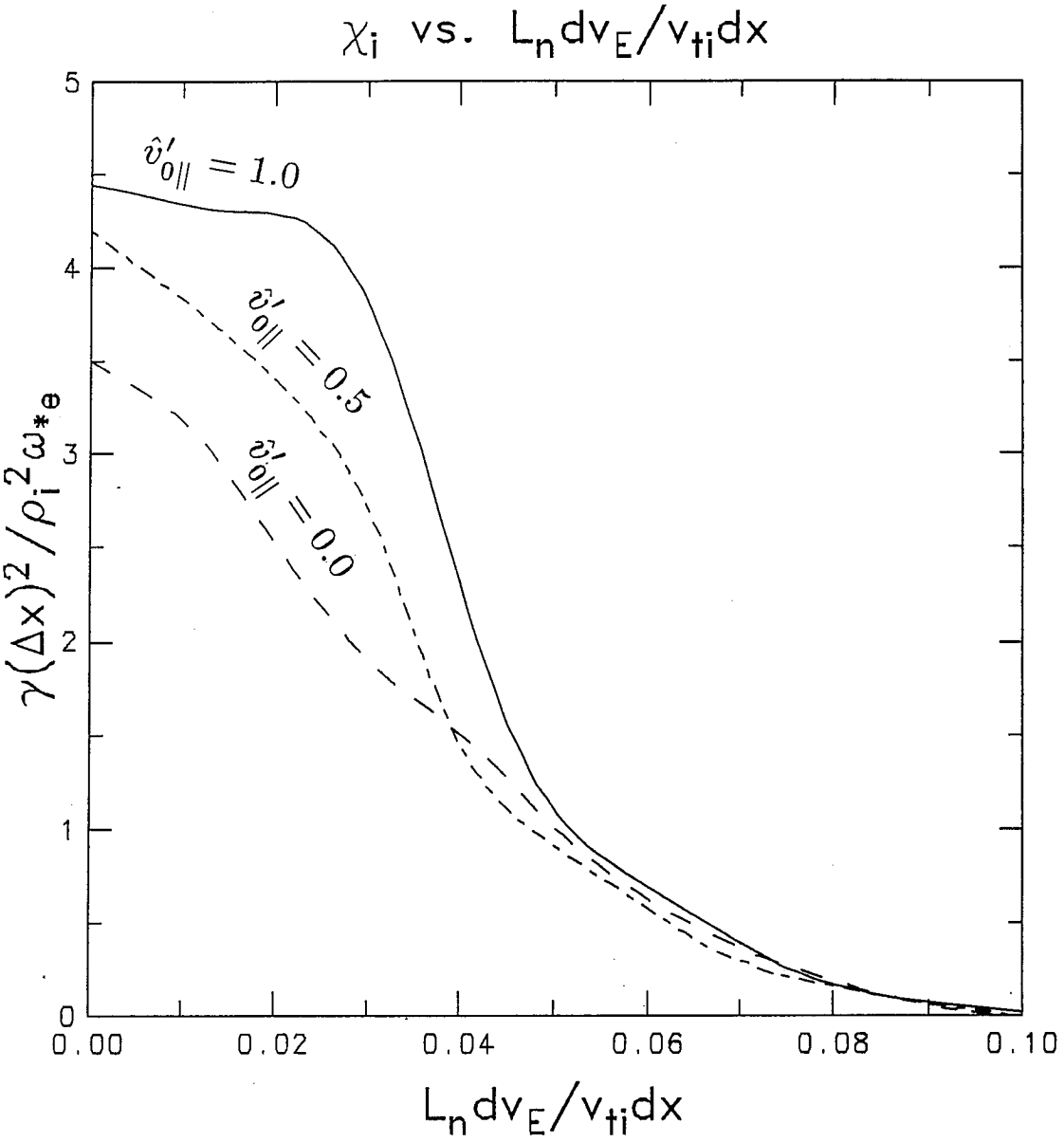
χ_i vs. $L_n dv_E/v_{ti}dx$
$\hat{v}'_{0\parallel} = 1.0$
$\hat{v}'_{0\parallel} = 0.5$
$\hat{v}'_{0\parallel} = 0.0$
$\gamma(\Delta x)^2/\rho_i^2\omega_{*e}$
0
1
2
3
4
5
0.00
0.02
0.04
0.06
0.08
0.10
$L_n dv_E/v_{ti}dx$

Fig. 10

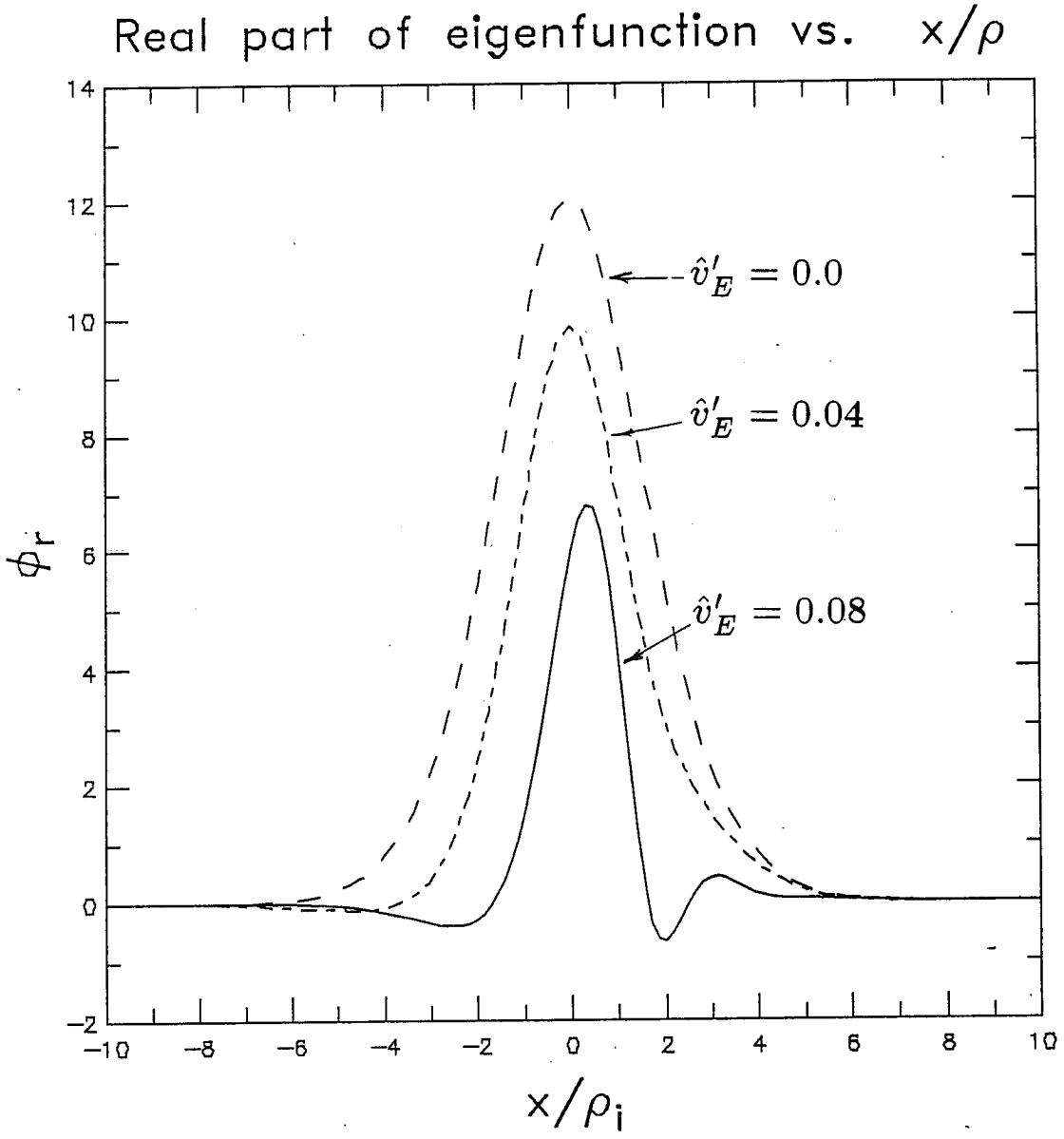
Real part of eigenfunction vs. x/ρ
14
12
10
8
6
4
2
0
−2
−10
−8
−6
−4
−2
0
2
4
6
8
10
ϕ_r
$\hat{v}'_E = 0.0$
$\hat{v}'_E = 0.04$
$\hat{v}'_E = 0.08$
x/ρ_i

Fig. 11

Table I

DIII-D Shear Flow Stability Parameters
Discharge #69785, $B = 2.1\,\mathrm{T}$, $I = 1.6\,\mathrm{MA}$, $R/a = 1.67\,\mathrm{m}/0.67\mathrm{m}$
deuterium $T_i \sim 200 - 600\,\mathrm{ev}$, $T_e \sim 100 - 250\,\mathrm{ev}$

Gradients	L	H
$\frac{dT_i}{dr}$	$-8.3\,\mathrm{kev/m}$	$-21.4\,\mathrm{kev/m}$
$\frac{dT_e}{dr}$	$-7.3\,\mathrm{kev/m}$	$-7.3\,\mathrm{kev/m}$
L_{Ti}	4.5 cm	2.1 cm
L_{Te}	2.4 cm	2.4 cm
L_n	3.4 cm	3.4 cm
L_s	80 cm	80 cm
$\frac{dv_E}{dr}$	$(2-4)\times 10^5\,/\mathrm{s}$	$(4-8)\times 10^5\,/\mathrm{s}$
$\frac{dv_\phi}{dr}$	$(1-5)\times 10^5/\mathrm{s}$	$(5-10)\times 10^5\,/\mathrm{s}$